Physiological Assessment of Coronary Stenoses and the Microcirculation

Javier Escaned
Justin Davies
Editors

Springer

Physiological Assessment of Coronary Stenoses and the Microcirculation

Javier Escaned
Justin Davies
Editors

Physiological Assessment of Coronary Stenoses and the Microcirculation

Springer

Editors
Javier Escaned
Hospital Clínico San Carlos
Universidad Complutense de Madrid
Madrid
Spain

Justin Davies
Imperial College London
London
UK

ISBN 978-1-4471-5244-6 ISBN 978-1-4471-5245-3 (eBook)
DOI 10.1007/978-1-4471-5245-3

Library of Congress Control Number: 2017940189

Printed on acid-free paper

This Springer imprint is published by Springer Nature
The registered company is Springer-Verlag London Ltd.
The registered company address is: 236 Gray's Inn Road, London WC1X 8HB, United Kingdom

Preface

This book was completed in 2016, when coronary physiology probably reached its maturity.

Forty years had passed since the publication of the landmark articles linking stenosis severity and coronary flow impairment. The impact of this research was enormous and triggered the development of numerous invasive and non-invasive technologies aimed at interrogating the coronary circulation with a new index, coronary flow reserve.

Twenty years later, fractional flow reserve (FFR) demonstrated its diagnostic utility as a pressure-derived index of stenosis severity. Over the next decades, FFR was used in clinical trials to demonstrate the importance of functional guidance of coronary revascularization and demonstrated, this time without any residual doubt, that angiography is a deceptive technique in assessing functional relevance of coronary stenoses.

Today, two decades later, a new revolution in coronary physiology is occurring applying computational fluid dynamics and in silico simulations to coronary imaging with the aim of calculating FFR-like indices without the need for intracoronary instrumentation. Furthermore, new indices such as the instantaneous wave free ratio (iFR) have been developed to facilitate easier pressure guidewire interrogation of the coronary arteries and hopefully increase its use.

Despite this progress and the growing interest generated by these developments, adoption of coronary physiology in clinical practice is still lagging. The main aim of this book is to serve both as an introduction to coronary physiology for all those interested in the field of cardiovascular disease and as a companion for practicing clinical and interventional cardiologists.

In that regard, this book provides a comprehensive approach to the interrogation of different domains of the coronary circulation. In 2016, coronary physiology is still largely stenosis centered. Assessment of the coronary microcirculation is seldom performed in the catheterization laboratory, and few centers routinely perform coronary vasomotion tests. This occurs despite growing information on the implications that microcirculatory and vasomotion disorders have for both patient's symptoms and prognosis. It is quite likely that a more extensive interest in these topics will foster the development and availability of diagnostic methods to interrogate the coronary circulation beyond the stenoses. And if this happens, surely new avenues for research and patient care will follow.

We are extremely grateful to all the authors for sharing their expertise in the topics covered in the many chapters of this book. We are also indebted to our Deputy Editors Hernán Mejía-Rentería, MD, and Nicola Ryan, MB, BCh, for their support throughout the edition of this book, and to Sara Fernández, MSc, for valuable technical assistance.

Madrid, Spain — Javier Escaned
London, UK — Justin Davies

Contents

V Indices of Coronary Resistance

VI Fractional Flow Reserve (FFR)

VII Instantaneous Wave Free Ratio (iFR)

VIII Multimodality Assessment of the Coronary Circulation

IX Wave Intensity Analysis

X Assessment of Endothelial Dysfunction

XI Research Models

Contributors

Diego Arroyo
Department of Cardiology
Fribourg University and Hospital
Fribourg, Switzerland

Sérgio Baptista
Hospital do Espírito Santo Évora
Evora, Portugal
sergio.b.baptista@gmail.com

Christopher J. Broyd
Interventional Cardiology Unit
Department of Cardiology
Hospital Clínico San Carlos
Madrid, Spain

Imperial College London
London, UK
c.broyd@imperial.ac.uk

Lorena Casadonte
Department of Biomedical Engineering and Physics
Academic Medical Center
University of Amsterdam
Amsterdam, The Netherlands
l.casadonte@amc.uva.nl

Carlos A. Collet
Cardiology
Academic Medical Center
Amsterdam, The Netherlands
carloscollet@gmail.com

Stéphane Cook
Department of Cardiology
Fribourg University & Hospital
Fribourg, Switzerland
stephane.cook@unifr.ch

Justin Davies
Imperial College London
London, UK
justindavies@heart123.com

Harry R. Davis
CVPath Institute, Inc
Gaithersburg, MD, USA

Pedro de Araújo Gonçalves
Hospital do Espírito Santo Évora
Evora, Portugal
paraujogoncalves@yahoo.co.uk

Guus A. de Waard
Department of Cardiology
VU University Medical Center
Institute for Cardiovascular Research
Amsterdam, The Netherlands
g.dewaard@vumc.nl

María Del Trigo
Interventional Cardiology Unit
Department of Cardiology
Hospital Clínico San Carlos
Madrid, Spain
mariadeltrigo@hotmail.com

Fernando Dominguez
Heart Failure and Inherited Cardiac Diseases Unit
Department of Cardiology
Hospital Universitario Puerta de Hierro
Madrid, Spain
fdominguezrodriguez@gmail.com

Dirk J. Duncker
Division of Experimental Cardiology
Department of Cardiology
Thoraxcenter
Erasmus MC
University Medical Center Rotterdam
Rotterdam, The Netherlands
d.duncker@erasmusmc.nl

Mauro Echavarría-Pinto
Interventional Cardiology Unit
Department of Cardiology
Hospital Clínico San Carlos
Madrid, Spain
mauroep@hotmail.com

Javier Escaned
Interventional Cardiology Unit
Department of Cardiology
Hospital Clínico San Carlos
Madrid, Spain
escaned@secardiologia.es

Aloke V. Finn
CVPath Institute, Inc
Gaithersburg, MD, USA
afinn@cvpath.org

Pablo Garcia-Pavia
Heart Failure and Inherited Cardiac Diseases Unit
Department of Cardiology
Hospital Universitario Puerta de Hierro
Madrid, Spain
pablogpavia@yahoo.es

Chrysafios Girasis
Department of Cardiology
Onassis Cardiac Surgery Center
Athens, FL, Greece
chrisgirasis@gmail.com

Nieves Gonzalo
Interventional Cardiology Unit
Department of Cardiology
Hospital Clínico San Carlos
Madrid, Spain
Nieves_gonzalo@yahoo.es

Ilkka H. A. Heinonen
Division of Experimental Cardiology
Department of Cardiology
Thoraxcenter
Erasmus MC
University Medical Center Rotterdam
Rotterdam, The Netherlands

Turku PET Centre
Turku, Finland

Department of Clinical Physiology and Nuclear Medicine
University of Turku and Turku University Hospital
Turku, Finland
ilkka.heinonen@utu.fi

Maurits R. Hollander
Department of Cardiology
VU University Medical Center
Amsterdam, The Netherlands
m.hollander@vumc.nl

Pilar Jiménez-Quevedo
Interventional Cardiology Unit
Department of Cardiology
Hospital Clínico San Carlos
Madrid, Spain
pjimenezq@salud.madrid.org

Michael Joner
CVPath Institute, Inc
Gaithersburg, MD, USA
joner@dhm.mhn.de

Morton J. Kern
Long Beach Veterans Affairs Medical Center
University of California
Irvine Medical Center
Long Beach, CA, USA
mkern@uci.edu

Frank D. Kolodgie
CVPath Institute, Inc
Gaithersburg, MD, USA

Antonio Maria Leone
Institute of Cardiology
Catholic University of the Sacred Heart
Rome, Italy
antoniomarialeone@gmail.com

Amir Lerman
Cardiovascular Institute Hospital Clínico San Carlos
Madrid, Spain
lerman.amir@mayo.edu

Fernando Macaya
Interventional Cardiology Unit
Department of Cardiology
Hospital Clínico San Carlos
Madrid, Spain
webjazzler@gmail.com

Koen M. Marques
Department of Cardiology
VU University Medical Center
Institute for Cardiovascular Research
Amsterdam, The Netherlands
km.marques@vumc.nl

Yasushi Matsuzawa
Cardiovascular Institute Hospital Clínico San Carlos
Madrid, Spain
matsuzawa-yuji@sumitomo-hp.or.jp

Hernán Mejía-Rentería
Interventional Cardiology Unit
Department of Cardiology
Hospital Clinico San Carlos
Madrid, Spain
hernan_m_r@yahoo.com

Daphne Merkus
Division of Experimental Cardiology
Department of Cardiology
Thoraxcenter
Erasmus MC
University Medical Center Rotterdam
Rotterdam, The Netherlands

Hiroyoshi Mori
CVPath Institute, Inc
Gaithersburg, MD, USA

David Neves
Hospital do Espírito Santo Évora
Evora, Portugal
dneves@hevora.min-saude.pt

Giampaolo Niccoli
Institute of Cardiology
Catholic University of the Sacred Heart
Rome, Italy
gniccoli73@hotmail.it

Sukhjinder Nijjer
Hammersmith Hospital
Imperial College Healthcare NHS Trust
London, UK
s.nijjer@yahoo.co.uk

Luis Nombela-Franco
Interventional Cardiology Unit
Department of Cardiology
Hospital Clínico San Carlos
Madrid, Spain
luisnombela@yahoo.com

Ivan Nuñéz-Gil
Interventional Cardiology Unit
Department of Cardiology
Hospital Clínico San Carlos
Madrid, Spain
ibnsky@yahoo.es

Peter Ong
Department of Cardiology
Robert-Bosch Krankenhaus
Stuttgart, Germany
Peter.Ong@rbk.de

Yoshinobu Onuma
Department of Cardiology, Erasmus Medical Center
Madrid, Spain
yoshinobuonuma@gmail.com

Kim Parker
Imperial College London
London, UK
k.parker@imperial.ac.uk

Ricardo Petraco
Imperial College London
London, Uk
r.petraco@imperial.ac.uk

Jan J. Piek
AMC Heart Centre
Academic Medical Centre
University of Amsterdam
Amsterdam, The Netherlands
j.j.piek@amc.nl

Serban Puricel
Department of Cardiology
Fribourg University & Hospital
Fribourg, Switzerland
serbanpurciel@icloud.com

Alicia Quirós
Interventional Cardiology Unit
Department of Cardiology
Hospital Clínico San Carlos
Madrid, Spain
alicia.quiros@unileon.es

Ruben Ramos
Hospital do Espírito Santo Évora
Evora, Portugal
ruben.a.b.ramos@gmail.com

Luís Raposo
Hospital do Espírito Santo Évora
Evora, Portugal
lfor.md@gmail.com

Vera Rodriguez
Interventional Cardiology Unit
Department of Cardiology
Hospital Clínico San Carlos
Madrid, Spain
verarodriguez@yahoo.com

Nicola Ryan
Interventional Cardiology Unit
Department of Cardiology
Hospital Clínico San Carlos
Madrid, Spain
nicolaryan@gmail.com

Giancarla Scalone
Institute of Cardiology
Catholic University of the Sacred Heart
Rome, Italy
gcarlascl@gmail.com

Udo Sechtem
Department of Cardiology
Robert-Bosch Krankenhaus
Stuttgart, Germany
Udo.Sechtem@rbk.de

Christian Seiler
Department of Cardiology
University Hospital
Bern, Switzerland
christian.seiler@insel.ch

Patrick W. Serruys
International Centre for Circulatory Health NHLI
Imperial College of London
Rotterdam, The Netherlands
Patrick.w.j.c.serruys@gmail.com

Arnold H. Seto
Long Beach Veterans Affairs Medical Center
University of California
Irvine Medical Center
Long Beach, CA, USA
Arnold.seto@va.gov

Murat Sezer
Istanbul Faculty of Medicine
Department of Cardiology
Istanbul University
Istanbul, Turkey
sezermr@gmail.com

Maria Siebes
Department of Biomedical Engineering and Physics
Academic Medical Center
University of Amsterdam
Amsterdam, The Netherlands
m.siebes@amc.uva.nl

Oana Sorop
Division of Experimental Cardiology
Department of Cardiology
Thoraxcenter
Erasmus MC
University Medical Center Rotterdam
Rotterdam, The Netherlands
o.sorop@erasmusmc.nl

Charles Taylor
Cardiovascular Institute Hospital Clínico San Carlos
Madrid, Spain
taylor@heartflow.com

Mario Togni
Department of Cardiology
Fribourg University and Hospital
Fribourg, Switzerland
mario.togni@unifr.ch

Sabahattin Umman
Istanbul Faculty of Medicine
Department of Cardiology
Istanbul University
Istanbul, Turkey
ummans@e-kolay.net

Luis Felipe Valenzuela-García
Cardiovascular Institute Hospital Clínico San Carlos
Madrid, Spain
lfvgmjrh1@yahoo.es

Tim P. van de Hoef
AMC Heart Centre
Academic Medical Centre
University of Amsterdam
Amsterdam, The Netherlands
t.p.vandehoef@amc.uva.nl

Nina W. van der Hoeven
Department of Cardiology
VU University Medical Center
Amsterdam, The Netherlands
ni.vanderhoeven@vumc.nl

Niels van Royen
Department of Cardiology
VU University Medical Center
Institute for Cardiovascular Research
Amsterdam, The Netherlands
n.vanroyen@vumc.nl

Renu Virmani
CVPath Institute, Inc
Gaithersburg, MD, USA
rvirmani@cvpath.org

Nicolaas Westerhof
Department of Cardiology
VU University Medical Center
Institute for Cardiovascular Research
Amsterdam, The Netherlands
n.westerhof@vumc.nl

The Physiology of the Coronary Circulation

Contents

Hemodynamic Effects of Epicardial Stenoses

Lorena Casadonte and Maria Siebes

J. Escaned, J. Davies (eds.), *Physiological Assessment of Coronary Stenoses and the Microcirculation*,
DOI 10.1007/978-1-4471-5245-3_1

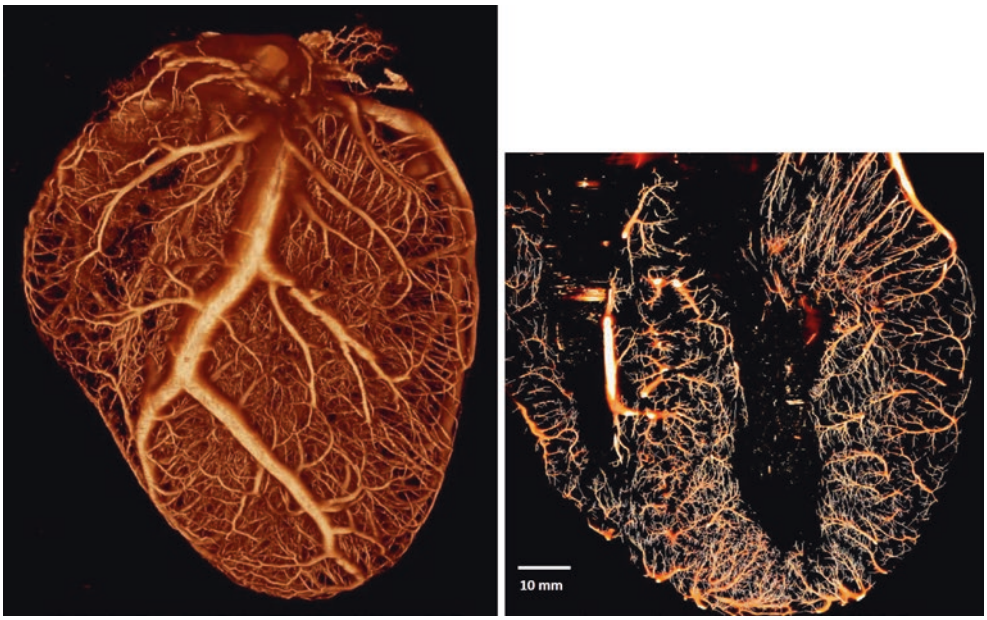

Fig. 1.1 3D image of coronary arteries of a dog heart obtained by a novel cryomicrotome technique with epifluorescence imaging. The vessels were filled with fluorescent cast material, and the frozen heart was alternately sliced at 40 μm and the bulk surface imaged with a high-resolution CCD camera [4]. The right panel shows a longitudinal cross section of a 2-mm-thick maximal intensity projection of transmural vessels (partially skeletonized) where the branching pattern of penetrating vessels is clearly visible

1.1 Principles of Coronary Physiology

A comprehensive understanding of coronary physiology is fundamental to aid in the interpretation of coronary pressure and flow signals obtained in patients with coronary artery disease. The heart is perfused by an intricate network of arteries that supply oxygen and nutrients to this continuously active muscle. Multiple branching vessels arise from epicardial conduit arteries (Fig. 1.1) and perfuse small volumes at the subepicardial layer of the myocardium, whereas the subendocardium is perfused by penetrating arteries that pass through the outer layers of the myocardium and only branch out into numerous vessels once they have reached the inner layer, where they supply larger volumes of myocardial tissue [1–4].

From a physical standpoint, minimal vascular resistance is principally determined by the segmental dimensions (length and diameter) of the distributed maximally dilated network. Thus, in the absence of epicardial coronary artery stenosis, maximal coronary flow is a function of the coronary driving pressure and of the maximal surface area of the dilated coronary resistance vessels. In this respect it is important to recall that all blood vessels are essentially elastic tubes when active smooth muscle tone is minimal. Once coronary arterioles are maximally dilated, they passively react to changes in distending and extravascular pressure, i.e., their diameter becomes pressure dependent [5–7].

Coronary pressure-flow relations Oxygen extraction from the coronary circulation is near maximal at rest, and raised myocardial oxygen demand is met by a corresponding change in coronary blood flow. The dynamic match to oxygen consumption at constant arterial pressure is denoted as metabolic flow adaptation or functional hyperemia. For a given cardiac workload, coronary blood flow remains constant over a wide range of arterial perfusion pressures (typically from about 60 to 140 mmHg) by an intrinsic mechanism denoted as autoregulation [8]. This entails coronary resistance changes in a direction parallel to the change in perfusion pressure. Importantly, autoregulation fails at higher pressures in subendocardial than subepicardial vessels [9, 10]. All arteries and arterioles contribute to flow control by changing their smooth muscle tone. Resistance to flow is negligible in large epicardial vessels, and most of coronary resistance resides in the intramural microvessels smaller than approximately 300 μm in diameter [11]. The regulation of coronary microvascular resistance includes integrative mechanisms of metabolic, myogenic, and flow-dependent vascular control, discussed in more detail elsewhere in this book. Distributed vasodilation decreases local microvascular resistance in the normal heart to maintain resting flow at the autoregulatory level as coronary pressure falls, e.g., in the presence of an epicardial coronary stenosis [12]. Substantial vasodilator reserve exists to increase flow above resting level during exercise, and values of 4–5 times above resting flow levels have been reported for humans [13–17]. Vasodilation results in a substantial redistribution of microvascular resistance compared to baseline conditions. Chilian and colleagues [11] reported that the resistance of arterial microvessels (<170 μm diameter) decreased nearly 15-fold for a sixfold increase in flow after dipyridamole administration, while papaverine caused preferential vasodilation of larger arterioles (>200 μm diameter) [18].

At low pressures the pressure-flow curve declines in a convex fashion toward the flow axis, and actual zero-flow pressure (P_{zf}) is only 2–4 mmHg above coronary sinus pressure at steady state [19]. The curvature reflects the progressive increase in resistance that results from the decrease in vascular transmural pressure. The curvilinear shape of this

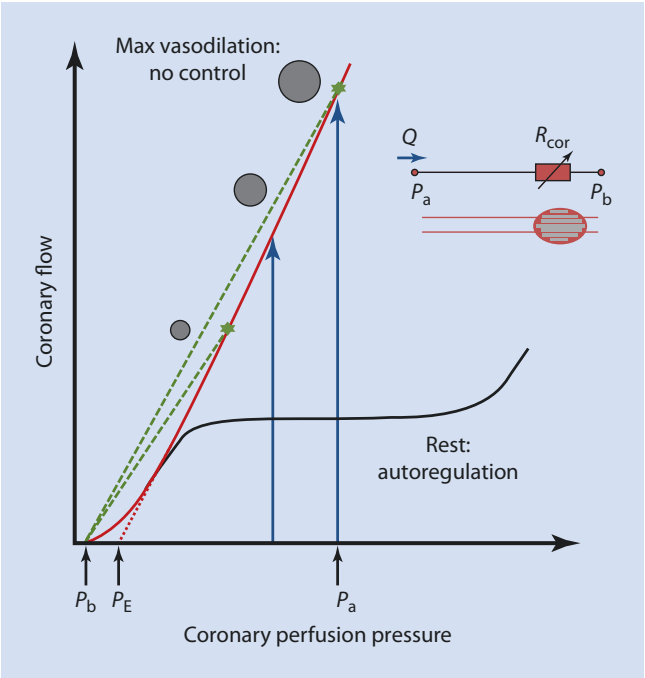

Fig. 1.2 Coronary pressure-flow relations in the absence of a stenosis. At rest, flow (*Q*) is maintained over a large range of arterial perfusion pressures. At maximal vasodilation (*red line*), flow can increase 4–5 times at normal arterial pressure (P_a); however, control is exhausted and flow reserve depends on pressure (blue arrows). The line curves at low pressures toward a zero flow intercept, which is the effective back pressure (P_b) to flow and only slightly above venous pressure. P_E is obtained by linear extrapolation of the straight part of the pressure-flow curve. As pressure falls, the diameter of the passive resistance vessels decreases (*circles*), and microvascular resistance (R_{cor}) gradually increases. The *dashed lines* (*green*) indicate pressure-flow lines at constant minimal resistance, shown here for a normal and a reduced perfusion pressure (*stars*). The inverse of the slope of these lines represents minimal resistance

pressure-flow curve is important in defining coronary vascular resistance, and the influence of distributed capacitive effects should be kept in mind when approximating zero-flow pressure by linear extrapolation to the pressure axis from data obtained after cessation of flow in epicardial vessels [19]. Moreover, data in isolated maximally dilated dog hearts suggest that P_{zf} is likely distributed across the left ventricular wall rather than being a function of global flow [20].

Typical coronary pressure-flow relations at autoregulation and at maximal vasodilation are schematically shown in Fig. 1.2.

The coronary pressure-flow relation at maximal vasodilation is a steep line with a nonzero pressure intercept, and flow is now a function of perfusion pressure. Although the pressure-flow curve at vasodilation (without control) appears relatively straight at pressures above about 40 mmHg, this line is likely the result of interacting mechanisms which are obscured from signals obtained at the epicardial arteries [21]. These include time constants involved in emptying microvascular compliance and coronary resistance changes that are affected by the greater narrowing of microvessels at the lower pressure range due to the strong nonlinear pressure-distensibility relation for vessels with relaxed smooth muscle tone [6, 22–26].

Coronary blood flow is principally determined by the driving pressure and the resistance of the coronary vascular bed. In the absence of an epicardial stenosis, the driving pressure is the difference between aortic input pressure P_a and the effective back pressure P_b at which flow becomes zero. Since steady-state P_b is difficult to assess in humans, venous pressure can be used as a reasonable approximation. In equivalence to Ohm's law, the resistance *R* of a vascular compartment is defined as the pressure drop ΔP across that compartment divided by flow *Q*:

$$R = \Delta P / Q \qquad \textbf{(1.1)}$$

By analogy, coronary resistance at vasodilation is then the inverse slope of the line connecting P_b on the pressure axis with the data point on the pressure-flow line at a certain arterial pressure (star symbol in Fig. 1.2). The decreasing slope of these lines reflects the increased coronary resistance at lower perfusion pressure, e.g., distal to a stenosis.

At vasodilation, coronary pressure and flow are *not* linearly related and do not pass through the origin. The intercept on the pressure axis makes this relation incremental linear, and the change in flow is not proportional to the change in pressure [26, 27]. Hence, the inverse slope of the hyperaemic pressure-flow line is not a measure of coronary resistance. Although the units are those of resistance, the inverse slope is the change in pressure divided by the *change* in flow. For example, the parallel rightward shift of this relationship from the arrested to the beating heart [28] clearly implies an increase in resistance due to cardiac contraction, but resistance determined from the slope would remain constant. Minimal coronary resistance has been shown to increase with decreasing perfusion pressure (and vice versa) in animals and humans [5, 6, 29, 30], and models that assume a pressure-independent microvascular resistance at maximal dilation are rather unrealistic.

Other influences can independently alter the coronary pressure-flow relationships illustrated schematically in Fig. 1.3.

An increase in oxygen consumption at rest shifts the autoregulatory plateau upward (1), which implies that autoregulation fails at higher pressure. Additionally, an increased resistance with lower maximal flow at the same pressure ensues when the slope of the pressure-flow relation for maximally dilated vessels decreases (2), as with left ventricular hypertrophy, increased blood viscosity in polycythemia, or small vessel disease due to, e.g., hypertension [31, 32]. Notably, a rise in myocardial wall stress due to cardiac contraction induces a rightward shift of the hyperemic pressure-flow curve. This parallel shift between a non-beating and a beating heart was shown to amount to half of the mean left ventricular pressure [26, 28]. Several other factors can raise zero-flow pressure (3), such as elevated left ventricular end-diastolic pressure or coronary venous pressure [33, 34], and collateral flow, which tends to decrease the curvature at the low-pressure range [35, 36]. It is possible for several factors to operate

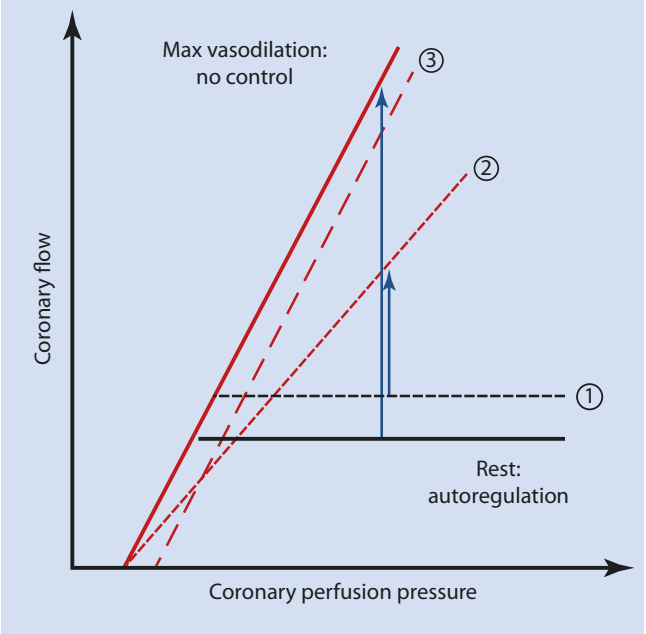

Fig. 1.3 Factors that decrease coronary flow reserve at any perfusion pressure. (*1*) A raised autoregulated flow, e.g., due to increased oxygen consumption. (*2*) When the slope of the pressure-flow line during maximal vasodilation is reduced, the maximum flow falls. (*3*) A parallel shift to the right of the pressure-flow relationship during vasodilation increases zero-flow pressure. Note that autoregulation fails at higher pressures for each condition

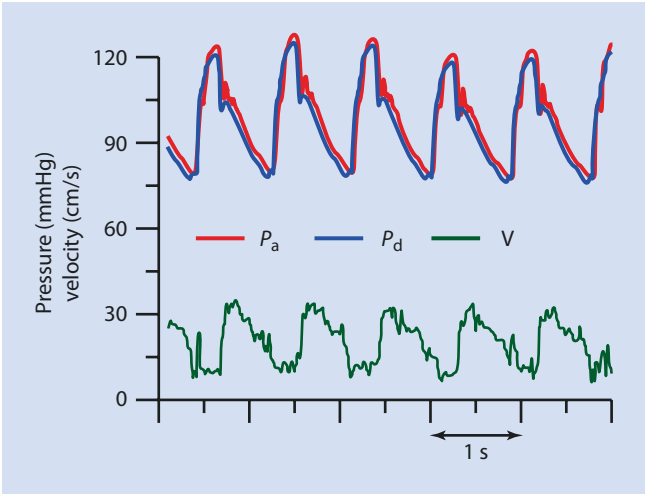

Fig. 1.4 Typical pressure and flow velocity waveforms obtained in a normal coronary artery at rest. Coronary flow is maximal during the diastolic phase. P_a aortic pressure, P_d distal coronary pressure, *v* flow velocity

synergistically, leading to a more pronounced reduction in flow reserve for any given perfusion pressure and to failure of autoregulation at a higher pressure. These concepts have been summarized in several publications [10, 26, 32, 37, 38].

Determinants of coronary blood flow The main cause for the pulsatile behavior of coronary blood flow is cardiac contraction. In contrast to the systemic circulation, coronary inflow is low in systole despite higher input pressure and highest in diastole when aortic input pressure declines (Fig. 1.4).

The forces exerted by the squeezing action of the heart muscle on the compressible vessels embedded in the myocardium vary the intramural blood volume throughout a heartbeat and lead to an impediment of systolic inflow and augmentation of venous outflow during systole. The out-of-phase behavior of these signals can be explained by the intramyocardial pump model [22, 23, 39] and varying elastance concept [40]. Basically, the transmural tissue pressure gradient generated by the intramyocardial pump that acts on the intramyocardial compliance is modulated by the time-varying elastance of the myocardium and vessels during the cardiac cycle [25, 41]. Both models assume that coronary resistance is volume dependent. The distensibility of the intramural vessels in interaction with the surrounding myocardial tissue constitutes the so-called intramyocardial compliance. The rate of volume exchange between systole and diastole (capacitive flow) modifies the microvascular inflow and outflow resistances [42, 43]. Due to the longtime constants involved in changing the blood volume of the large intramyocardial compliance, microvascular resistance is varying throughout the cardiac cycle and cannot simply be divided into systolic and diastolic components.

Transmural flow and subendocardial vulnerability A dense network of branching elastic vessels delivers blood flow across the myocardium; however, the flow distribution across the myocardium is not uniform. Studies in animals and humans have demonstrated a profound perfusion heterogeneity both across and within layers [44–46], which makes it difficult to assess subendocardial perfusion from epicardial intracoronary measurements.

Several mechanisms contribute to the subendocardial vulnerability to ischemia [47]. The impeding effect of extravascular compression during cardiac contraction is stronger at the subendocardium. This is partially compensated by the larger total volume of the resistance vessels in the inner than the outer layer of the heart wall, yielding a lower intrinsic resistance at full dilation [48]. Subendocardial perfusion was shown to be about 50 % higher than at the subepicardium in the non-beating dog heart [2]. Transmural perfusion during maximal coronary vasodilation was nearly uniform at a heart rate of 100 bpm, whereas subendocardial flow was about half of subepicardial flow at a heart rate of about 200 bpm [49]. This implies that over heart rates ranging from 0 to 200 bpm, heart contraction may reduce subendocardial flow by a factor of 3, while subepicardial flow may even slightly increase at elevated heart rates [50].

Clearly, factors that affect the rate of filling of intramural vessels in diastole, such as perfusion pressure and the duration of diastole [51], modulate microvascular conductance at the subendocardium. Perfusion pressure is generally lower in the subendocardial layer due to the longer path length (greater longitudinal pressure drop) for blood to reach the subendocardium via transmural penetrating vessels. A decreased perfusion pressure tends to redistribute blood flow

away from the subendocardium and causes a reduction of the subendocardial/subepicardial blood flow ratio [52]. Further reduction in perfusion pressure distal to a stenosis decreases the diameter of subendocardial arterioles more than the subepicardial arterioles, and additionally, a stenosis selectively decreases the dilatory response of subendocardial arterioles [53]. Another confounding factor is inadequate perfusion time, expressed as the diastolic time fraction, DTF, which leads to insufficient flow to subendocardium, while the more superficial layers may still be adequately perfused. Moreover, the effect of DTF on subendocardial blood flow is exacerbated at low perfusion pressure distal to a stenosis [54–56]. Interestingly, DTF was shown to be prolonged at reduced coronary pressure distal to a stenosis, which may act as a protective regulatory mechanism when vasodilatory reserve is exhausted [57].

1.2 Stenosis Hemodynamics

This section provides an overview of stenosis fluid dynamics and its mathematical description as derived from in vitro and in vivo experiments.

Stenosis pressure drop-flow (Δ*P*-*Q*) characteristics Pressure is lost due to viscous friction, when blood flows through a vessel. For steady and laminar flow, the pressure drop ΔP over a uniform tube of length L is given by Poiseuille's law as

$$\Delta P = \frac{32\ \mu L}{D^2} v \tag{1.2}$$

where μ is the viscosity, D is the diameter of the tube, and v is the mean cross-sectional velocity. In terms of volume flow Q and diameter D, this equation becomes

$$\Delta P = \frac{128\ \mu L}{\pi D^4} Q \tag{1.3}$$

This implies that for a given tube dimension and length, the resistance $R = \Delta P/Q$ is constant. Viscous shear determines viscous energy losses along the entire length of an artery. The pressure drop increases with the inverse fourth power of the tube diameter, i.e., when the diameter is reduced by factor of 2, the resistance increases 16 times for the same flow and unit length. This relationship clearly shows the dominant influence of vessel diameter, and both active and passive mechanisms can substantially change vessel resistance and flow.

The main assumptions for Poiseuille's law are (1) a rigid, straight tube of uniform cross section, (2) steady, laminar flow with a parabolic velocity profile, and (3) constant viscosity, i.e., blood is considered a Newtonian fluid. These assumptions are far from true in curved, branching, and compliant vessels with pulsatile blood flow, but Poiseuille's law can serve as a first-order approximation.

For a change in diameter along the tube, conservation of mass applied to fluid transport comes into play. Conservation of mass states that the volume of blood entering a vessel per unit time is equal to the rate at which it leaves the vessel. This is described by the so-called continuity equation, with A the cross-sectional area:

$$Q = A_1 v_1 = A_2 v_2 = \text{constant} \tag{1.4}$$

Bernoulli's law relates blood pressure to flow velocity v and is based on the conservation of energy and conservation of momentum. It states that the sum of static pressure, hydrostatic pressure (potential energy), and dynamic pressure (kinetic energy) remains constant:

$$P_{tot} = P + \rho g h + \tfrac{1}{2}\rho v^2 = \text{constant} \tag{1.5}$$

where ρ is the blood density, g is the gravitational acceleration, and h is the height of the fluid column above a reference level. Pressure losses due to friction are neglected (inviscid flow is assumed), and the fluid is considered incompressible, with constant density. Note that for a blood density of 1.06 g/cm^3, a difference in hydrostatic pressure (mmHg) is related to a change in the height (h, cm) by $\Delta P = \Delta h \cdot 0.78$. If the height is constant, then Eq. 1.5 reduces to

$$P_1 + \tfrac{1}{2}\rho v_1^2 = P_2 + \tfrac{1}{2}\rho v_2^2 \tag{1.6}$$

As blood enters a narrowed section, the velocity v increases proportional to the decrease in cross-sectional area of the vessel, and pressure is lost ($P_2 < P_1$) due to convective acceleration ($v_2 > v_1$), with conversion of pressure to kinetic energy, as depicted in Fig. 1.5. In addition, there is a pressure drop due to viscous losses as blood moves through the stenosis.

Under ideal circumstances, pressure would be recovered once the diverging section is reached where the flow decelerates. However, blood emerges from the stenosis as an inertial jet, leading to flow separation and formation of a recirculation zone, with eddies and viscous shear stresses between slow and fast moving fluid particles. The extent of this recirculation zone depends on stenosis area reduction and varies with flow [58, 59]. In addition, significant irreversible losses are incurred due to viscous friction along the length of the converging and narrowed section, which can be approximated by Poiseuille's law for the reduced diameter in the narrowed section. As a result, pressure is lowest inside the narrowed stenosis section, close to the point of flow separation, and only a small portion of kinetic energy is converted back to pressure energy downstream of the stenosis.

Based on a series of experiments with steady and pulsatile flows through models of concentric and eccentric stenoses in the 1970s, Young and co-workers [60–62] developed an empirical relationship describing the pressure drop across as a function of stenosis geometry. In essence, the total pressure drop across a stenosis is a quadratic function of flow and equals the sum of viscous losses along the entrance and throat of the stenosis, ΔP_v, that are linearly related to flow and inertial losses at the exit of the stenosis, ΔP_e, that scale with the square of the flow:

$$\Delta P = \Delta P_v + \Delta P_e \tag{1.7}$$

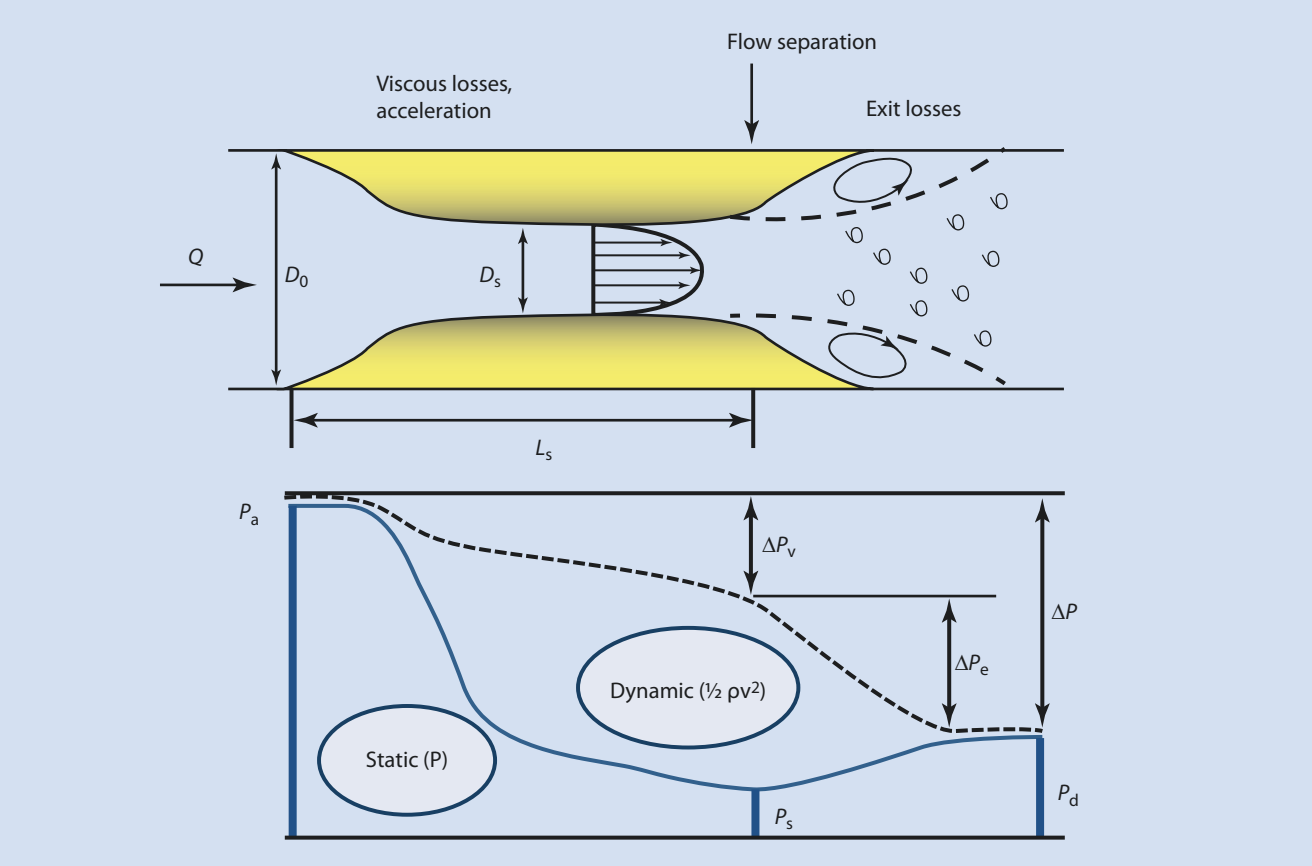

Fig. 1.5 Stenosis flow field (*top*) and energy loss (*bottom*). Pressure is lost by viscous friction along the converging and narrowed section. The convective acceleration due to diameter reduction causes conversion from static pressure energy to kinetic energy, with minimal pressure close to the point of flow separation. Exit losses are incurred at the expansion zone where the high-velocity jet leaving the narrowed section leads to formation of eddies and energy is converted to heat. The total pressure drop (ΔP) is the sum of viscous losses (ΔP_v) that scale linearly with flow and exit losses (ΔP_e) that increase with the square of flow. D_0 *and* D_s normal and stenosis diameter, resp., L_s length of converging section and throat up to the point of flow separation, Q flow rate, P_a aortic input pressure, P_s minimal stenosis pressure, P_d distal pressure, v velocity, ρ fluid density

Or expressed in terms of flow, Q

$$\Delta P = AQ + BQ^2 \tag{1.8}$$

where A and B are constants that derive from stenosis geometry and rheological properties of blood:

$$A = 32\frac{L_s}{D_0}\left(\frac{A_0}{A_s}\right)^2\frac{\mu}{A_0 D_0} \tag{1.8a}$$

$$B = \frac{\rho}{2}\frac{k_e}{A_0^2}\left(\frac{A_0}{A_s}-1\right)^2 \tag{1.8b}$$

where k_e is an exit coefficient that was originally determined to average 1.52 for blunt-ended stenoses with L_s/D_0=2 [60]. A series of additional experiments in the 1980s [63, 64] has shown that not only the stenosis area reduction A_0/A_s and length L_s but also the shape of the entrance and exit sections influence the overall pressure drop by altering the velocity profile as it develops along the entrance and throat of the constriction. This boundary-layer growth from the inlet to the outlet of a stenosis could empirically be accounted for by adjusting L_s/D_0 in Eq. 1.8a to

$$L_s'/D_0 = 0.45 + 0.86\left(L_s/D_0\right) \tag{1.8c}$$

and by expressing the exit loss coefficient k_e in Eq. 1.8b as a function of L_s/D_0:

$$k_e = 1.21 + 0.08\left(L_s/D_0\right) \tag{1.8d}$$

The gradually changing area reduction along the stenosis can be taken into account by integration of differential viscous losses over the stenosis length. The effect of the stenosis entrance region was also more recently investigated by Huo et al. [65] who proposed a second-order polynomial to determine the diffusive energy loss coefficients for different uniform (blunt/parabolic) velocity profiles at the entrance and outlet region.

Because resistance is per definition equal to pressure drop divided by the flow, Eq. 1.8 implies that stenosis resistance is given by

$$R_S = A + BQ \tag{1.9}$$

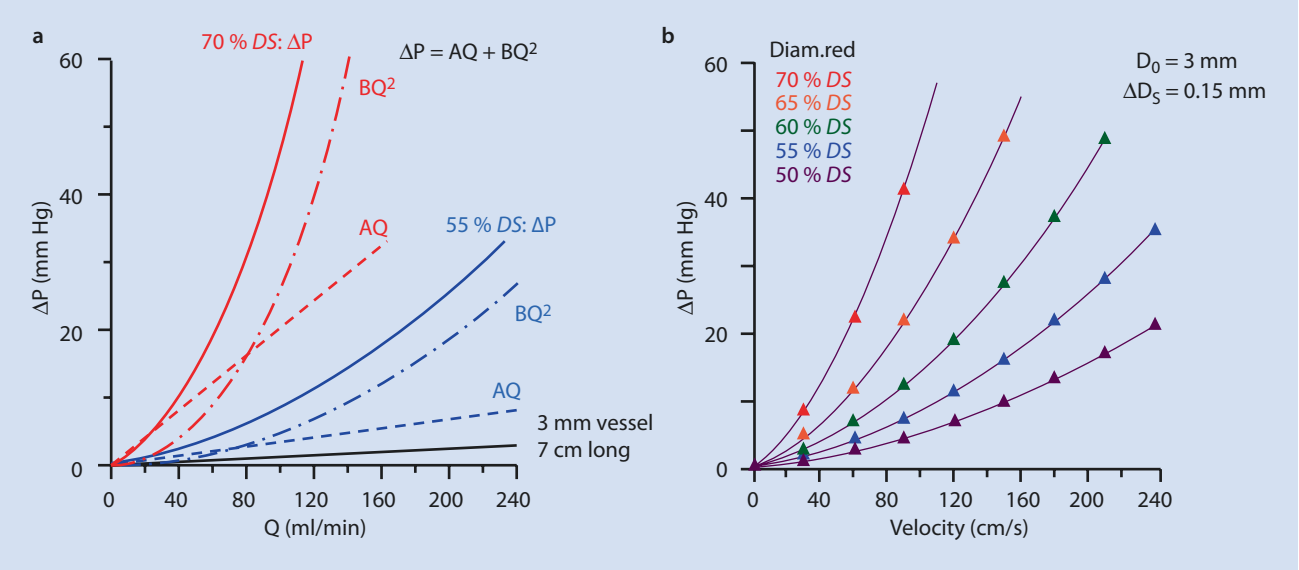

Fig. 1.6 Illustrations of stenosis pressure drop-flow relationship. **a** The total pressure gradient (ΔP) is the sum of linear viscous pressure losses (AQ) and quadratic exit losses (BQ^2). Theoretical relationships are shown for a 55 % and a 70 % diameter stenosis in a 3-mm vessel. The lower black line indicates pressure loss in the unobstructed vessel. **b** Effect of small changes in stenosis diameter (ΔD_s) in a vessel with 3-mm normal diameter (D_0). The pressure drop for a given flow rate increases progressively with each reduction in stenosis diameter by 0.15 mm

The first term on the right represents the viscous resistance which is constant for a given stenosis geometry, and the second term relates to exit losses that increase with flow.

The two additive components of stenosis pressure drop (Eq. 1.7) are graphically shown in Fig. 1.6a for a moderate and severe lesion with $L_s/D_0 = 2$ in a 3-mm vessel. Note that viscous losses dominate at low flow rates, while the nonlinear exit losses grow more quickly with increasing flow through the stenosis and makes up the larger contribution to the total pressure drop at elevated flow. The major geometric factor is the minimum stenosis diameter, which enters with its inverse fourth power into both terms of the ΔP-Q relationship. Even small changes in stenosis dimensions can have a large effect, as is illustrated in Fig. 1.6b. The difference between the ΔP-Q curves stems from a reduction in stenosis diameter by <0.2 mm, which produces a progressively larger incremental rise in pressure drop with increasing stenosis severity, even for moderate flow. This example highlights the influence of a small thrombus in the narrowed section, or the effect of passive changes in stenosis dimensions with variations in intraluminal pressure when a compliant plaque or wall section is present (see below).

The mean value of pulsatile flow (time averaged over a cardiac cycle) was shown to differ less than 5 % from the steady-state value in the coronary circulation [62, 65], and the general quadratic equation relating pressure drop to flow (Eq. 1.8) is applicable to both steady and pulsatile flow. Studies of coronary stenoses in unsedated dogs have shown that throughout diastole and mid-systole, the measured instantaneous data followed the theoretical form and that inertial effects due to rapid flow deceleration and acceleration during the cycle were limited to brief periods at the end of systole and beginning of diastole [66]. The general form of Eq. 1.8 has been used to derive hemodynamic characteristics of coronary artery stenoses in patients based on per-beat averages of pressure drop and flow velocity throughout the hyperemic response to a vasodilator stimulus [67]. Stenosis pressure drop-velocity relations also served to successfully assess hemodynamic stenosis severity by evaluating the pressure gradient at a fixed flow velocity of 50 cm/s for instantaneous diastolic flow and at 30 cm/s for cycle-averaged flow velocity [68, 69]. The advantage of this approach is that maximal vasodilation is not required (e.g., contrast injection can be used to increase flow), and potential pitfalls of baseline measurements associated with autoregulation or measurement errors are avoided.

1.3 Effects of Stenosis on Coronary Blood Flow

As outlined above, maximum myocardial perfusion depends on the sum of all resistances, and distal coronary pressure is the major determinant of microvascular perfusion. An epicardial stenosis represents an additional resistance to flow in the coronary system (Fig. 1.7). It is important to realize that stenosis resistance is directly dependent on flow and hence is variable, even for a stenosis of fixed geometry. Moreover, coronary microvascular resistance includes an active component governed by mechanisms of flow control and a passive component that is pressure dependent and determines minimal resistance of the dilated vessels without tone. Hence, all resistances are variable and functions of flow and pressure.

The hemodynamic effect of an epicardial stenosis in the context of coronary perfusion is schematically illustrated in Fig. 1.8, where the stenosis ΔP-Q relationship is combined with the pressure-flow relations of the coronary circulation at rest and at maximal vasodilation. The x-axis represents (distal) coronary perfusion pressure, and flow is shown on the y-axis.

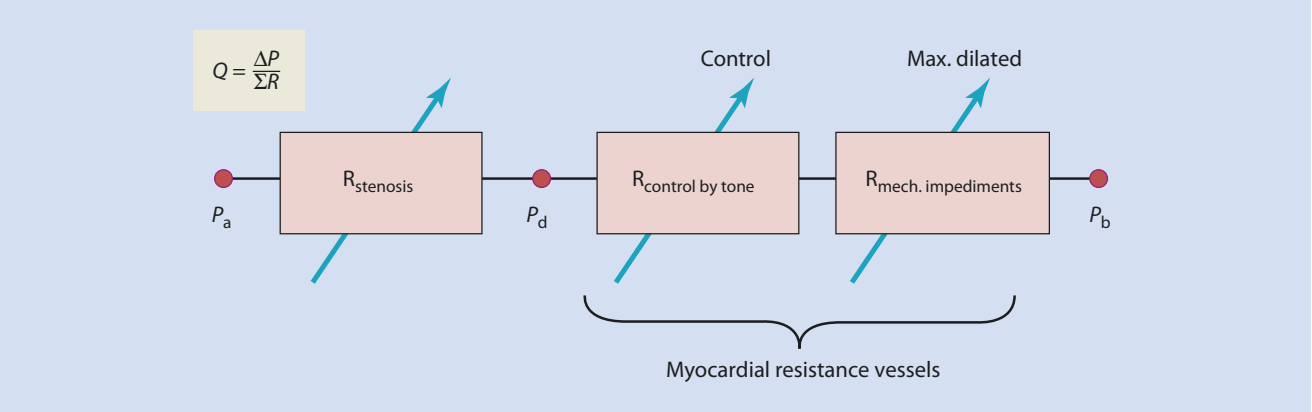

Fig. 1.7 Stenosis resistance is in series with microvascular resistance. Flow (Q) in a stenosed artery is determined by the total pressure gradient ($\Delta P = P_a - P_b$) divided by the sum of all resistances. Myocardial resistance vessels include a resistance that is controlled by tone and a minimum resistance at maximal vasodilation that is determined by the structure of the vascular tree and altered by mechanical impediments. P_d is the perfusion pressure for the microcirculation downstream of the stenosis. Note that all resistances are variable

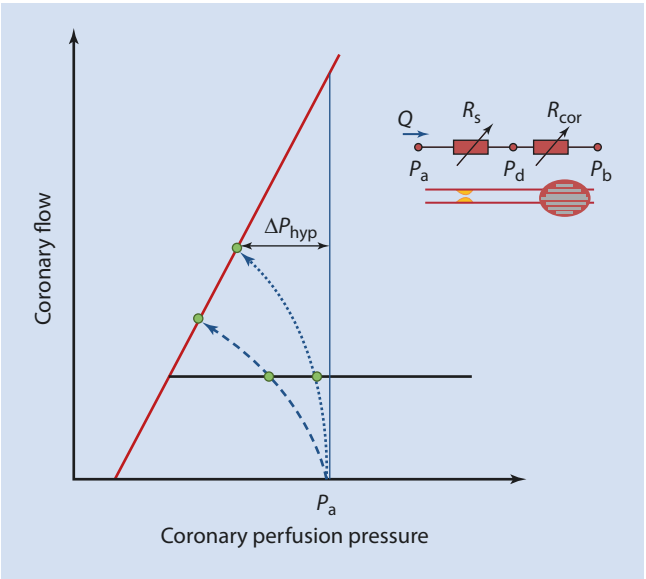

Fig. 1.8 Coronary pressure-flow relation and stenosis pressure drop-flow relations (*dashed lines*) shown for two stenoses of different severities. While the pressure drop at rest is compensated by a reduction in microvascular resistance, maximal flow is reduced with increasing stenosis severity (*dotted vs. dashed curve*), with an increase in hyperemic pressure drop (ΔP_{hyp})

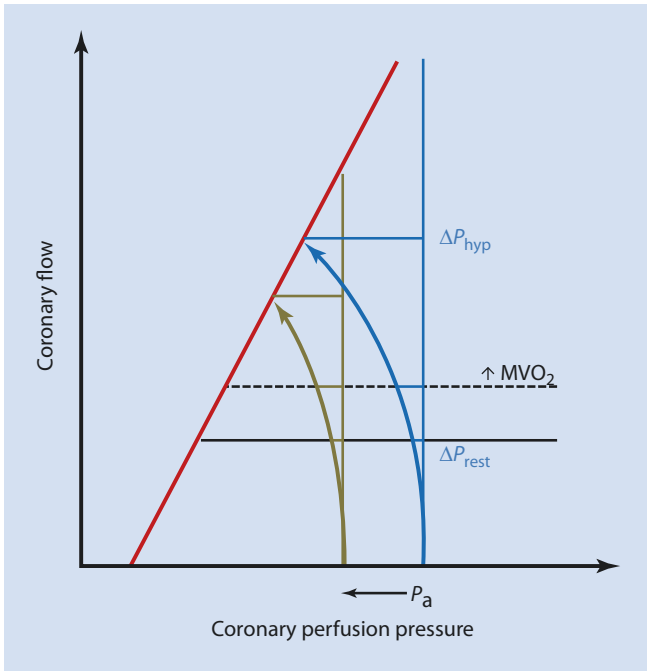

Fig. 1.9 Effect of decreasing perfusion pressure and increased resting flow on stenosis resistance for a given stenosis. The stenosis pressure drop-flow relation shifts to the left (*blue to brown*) when aortic pressure is reduced (P_a). The hyperemic pressure gradient (ΔP_{hyp}) is reduced because of a lower maximal flow that can be achieved, while pressure gradient at baseline (ΔP_{rest}) is unchanged. However, when resting flow is increased due to a higher oxygen consumption (MVO_2), resting pressure gradient is increased, while hyperemic pressure gradient is not affected. Note that stenosis resistance increases linearly with flow ($R_s = A + BQ$)

Starting from no-pressure drop at no flow ($P_d = P_a$), the curve representing stenosis pressure drop as a function of flow (Eq. 1.8) turns left toward lower distal perfusion pressure with increasing flow, reflecting the nonlinear loss in pressure across the stenosis with increasing flow. In order to maintain baseline flow at rest, the coronary microcirculation adapts to the presence of a stenosis and compensates for the additional pressure loss by lowering microvascular resistance, which in turn reduces the vasodilatory reserve. The maximal flow value is prescribed by the pressure-flow line at maximal vasodilation, which can turn downward or shift to the right in certain cardiovascular conditions, as discussed earlier. The difference between aortic pressure and the intersection with the hyperemic pressure-flow line is the stenosis pressure drop at maximal dilation.

If oxygen demand increases at rest, the intersection with the autoregulation plateau occurs at a higher flow (Fig. 1.9), which on fluid dynamic principles implies an increase in basal stenosis resistance commensurate with the nonlinear relationship between flow and stenosis pressure drop. Conversely, a

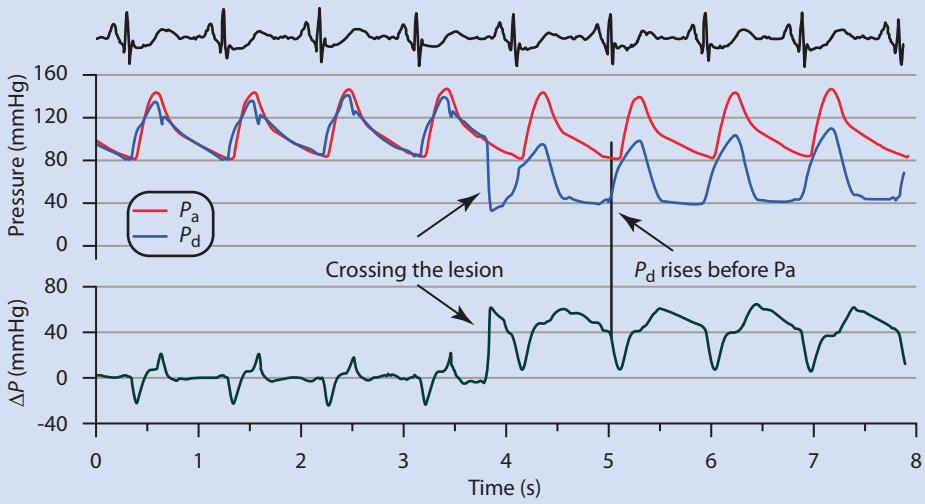

Fig. 1.10 Phasic tracings of aortic (P_a) and distal pressure (P_d) obtained in a patient's left anterior descending artery with a 75 % diameter stenosis. As the stenosis is crossed, a substantial pressure gradient (ΔP) is clearly seen that is higher during diastole. The distal pressure profile resembles a left ventricular pressure pattern. Note that coronary pressure downstream of the stenosis rises slightly before aortic pressure

decrease in aortic pressure will shift the pressure drop-flow relationship of this stenosis to the left resulting in a lower maximal flow, despite the same baseline resistance. Both examples entail a reduced capacity to increase flow above resting levels.

Effect of stenosis on pulsatile flow and pressure signals Development of an epicardial stenosis has a profound effect on pulsatile pressure and flow waveform patterns. An example obtained in a patient with a severe lesion (Fig. 1.10) shows how the pressure signal changes from an aortic to a ventricular pattern (not unlike that of the intramyocardial pump model) as the stenosis is crossed. This is explained by the higher diastolic flow and corresponding higher pressure loss during this part of the cardiac cycle. Note that the rise in distal pressure occurs earlier than the rise in aortic pressure. It is known from animal studies that distal pressure starts to increase during isovolumic contraction, whereas the pressure proximal to the stenosis rises with aortic pressure at the onset of aortic valve opening.

The availability of sensor-equipped guidewires allows the simultaneous acquisition of pulsatile coronary pressure and flow velocity data in patients. Figure 1.11 shows an example of coronary hemodynamic signals obtained in a left circumflex vessel with a severe lesion during increasing flow induced by intracoronary administration of adenosine, before (left) and after (right) percutaneous coronary intervention. In the presence of the stenosis, the distal pressure signal clearly reveals the hemodynamic stenosis severity. Although only a small increase in average flow velocity was attained during hyperemia (from 20 to 31 cm/s), the predominantly diastolic pressure gradient is exacerbated, with additionally a substantial pressure gradient during systole. Conversely, after revascularization, the distal pressure profile hardly changes despite a large rise in flow velocity (from 23 to 75 cm/s). The corresponding ΔP-Q relationships (lower panel) unequivocally illustrate the improvement in stenosis hemodynamics that was accomplished by revascularization, and the post-intervention ΔP-Q relationship closely approaches that obtained in an undiseased reference vessel of this patient. The solid lines represent least-squares quadratic fits through the data (Eq. 1.8). Note that the post-intervention and reference ΔP-Q relationships are almost straight, which indicates the dominance of viscous losses along the vessel (between the P_a at the ostium and the location of distal pressure sensor). This implies a lack of energy losses due to convective acceleration in a narrowed section (second term in Eq. 1.8) and confirms a successful hemodynamic outcome without further constrictions along the interrogated vessel path.

Compliant stenosis Pathological studies and intravascular imaging have shown that only a minority of coronary artery stenoses is concentric with a fixed, rigid geometry. Most plaques develop at the inner curvature of the epicardial vessel or at bifurcations, with a D-shaped, concentric, or elliptical residual lumen [70–73]. The eccentric location of the plaque implies that in most cases, an arc of normal wall circumference is present which provides a mechanism whereby variations in intraluminal pressure or vasomotor tone can affect the luminal dimensions and thus alter flow resistance. Moreover, the plaque itself can be compliant [74–77]. The hemodynamic significance of dynamic changes in stenosis dimensions has received much attention in the past, and both active and passive mechanisms have been demonstrated in vivo [78–85]. Especially when vasomotor tone of epicardial vessels is minimized after giving nitroglycerin, a passive change in stenosis geometry can take place during the hyperemic response, when flow velocity increases at the expense of intraluminal pressure in the narrowed section [67, 84]. For a stenosis with an arc of compliant wall, the decrease in pressure may lead to extra narrowing by partial passive collapse, thereby worsening the situation.

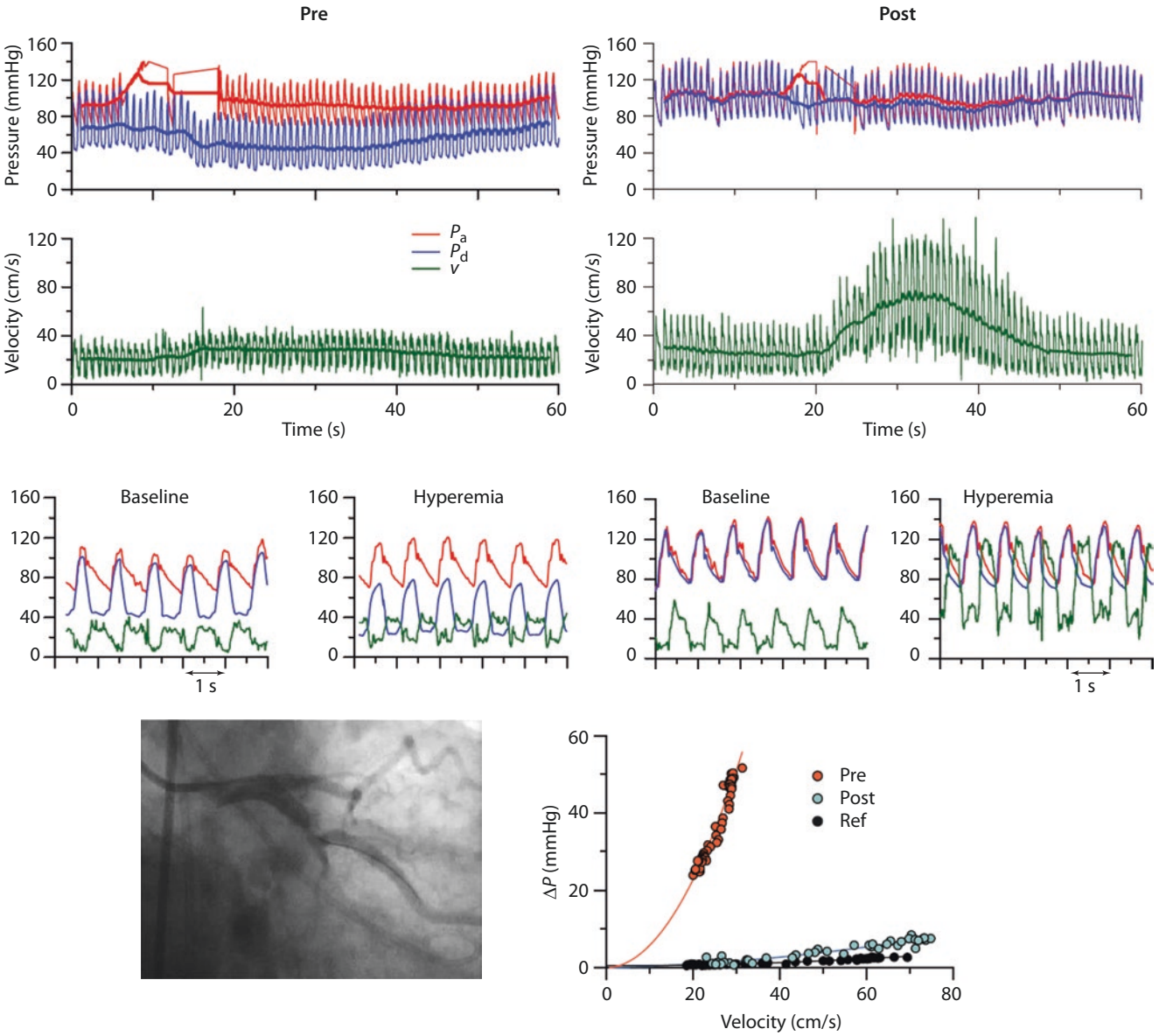

Fig. 1.11 Hyperemic response to an intracoronary adenosine injection. Simultaneous pressure and velocity measurements were obtained in a 63-year-old patient with a 85 % diameter stenosis in the left circumflex artery (angiogram) before (pre, *left*) and after (post, *right*) interventional revascularization. Middle panels show proximal (P_a) and distal (P_d) pressure and flow velocity (v) at baseline and maximal hyperemia for each condition. On the lower right, the corresponding pressure drop (ΔP)-velocity relations are shown for cycle-averaged values from baseline to hyperemia. Post intervention the ΔP-velocity relation closely approaches that of an undiseased reference vessel (Ref)

As outlined above (see Fig. 1.6b), even very small changes in minimum diameter can lead to large changes in pressure drop. In terms of the ΔP-Q relationship, stenosis hemodynamics is then no longer characterized by a single curve, but by a family of curves that reflect the changing stenosis geometry with time during the waxing and waning of flow [67]. The resulting ΔP-Q relationship of such a stenosis then displays in the form of a loop (Fig. 1.12), with two different pressure gradients at the same flow velocity, reflecting the passive dynamic change in stenosis dimensions.

Serial lesions Many lesions do not appear in isolation, but multiple stenoses are frequently present along a coronary artery. If the distance separating two lesions is sufficiently large, the overall pressure drop is simply the sum of the pressure drops across the individual stenoses. However, as the distance between the lesions decreases, interaction between the upstream and downstream lesion causes the overall pressure drop to be less than the sum. This interaction depends on the severity of the lesions, the distance between them, and the flow. At low flow rates, the expansion loss is small and two similar lesions act as a single lesion of summed length [60]. With increasing flow, two stenoses in series can undergo a transition from a single lesion of twice the length to two independent lesions with twice the overall pressure drop, as shown in Fig. 1.13. The flow rate at which this transition occurs decreases with increasing distance between the lesions, i.e., two lesions that are close together behave as a single lesion of twice

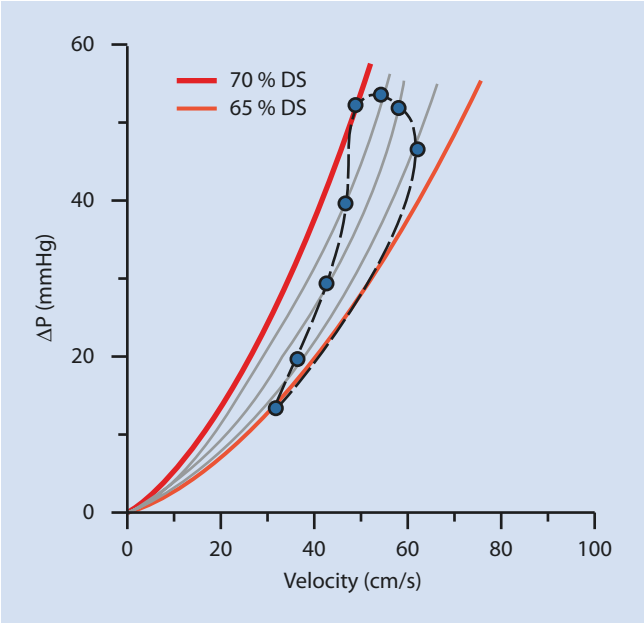

Fig. 1.12 Effect of stenosis compliance on the pressure drop (ΔP)-velocity relation. As intraluminal pressure declines with increasing velocity, partial collapse leads to a worsening of stenosis severity. The resulting loop is a composite of a family of unique curves that are traversed during the hyperemic response. Note that the change in stenosis geometry results in different pressure gradients for the same velocity

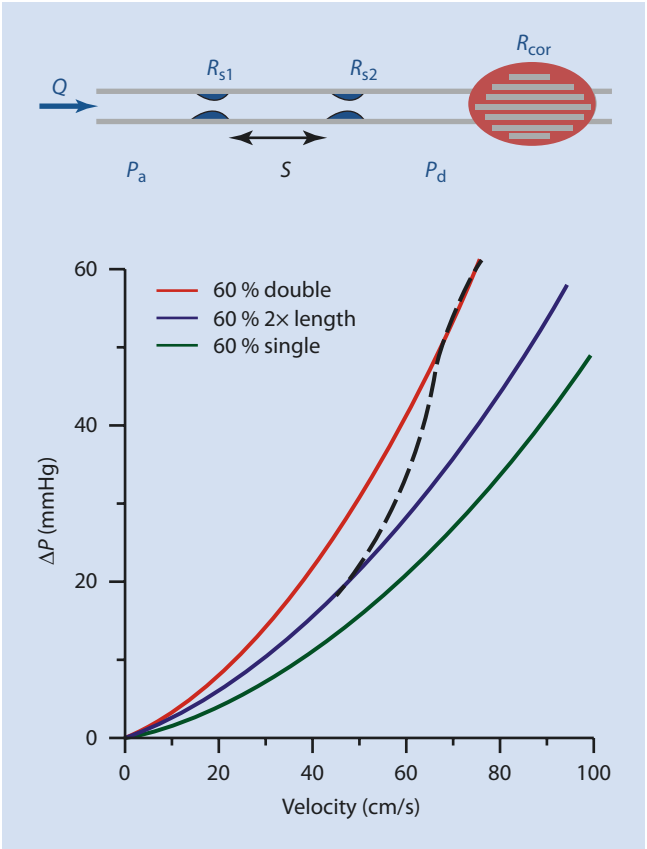

Fig. 1.13 Effect of two 60 % diameter stenoses in series on the pressure drop (ΔP)-velocity relation. A single stenosis is indicated by the *green line*. At low flow rates, two lesions act as a single lesion of twice the length (*blue line*). But with increasing flow, they undergo a transition (*dashed trajectory*) to two independent lesions with twice the pressure gradient (*red line*). This transition depends on the distance (S) between the lesions and on the sequence and severity of the stenoses. Q flow, R_s stenosis resistance, R_{cor} coronary resistance, P_a aortic pressure, P_d distal pressure

the length over a larger flow range compared to lesions that are further apart [86].

For a given flow rate, the "critical" separation distance for two lesions to act independently depends on stenosis severity and distance. This is in line with the extent of the flow expansion zone of the upstream stenosis mentioned earlier. If the jet leaving the proximal lesion can fully expand before the distal lesion is encountered, the lesions are fluid dynamically independent, and pressure loss is maximal. This reattachment length is longer at elevated flow and for more severe lesions (up to 5–10 normal diameters). Intermediate lesions (55 % diameter reduction) at moderate flow (physiological range) tended to act independently when the distance between the lesions, S, exceeding six times the normal diameter, i.e., when S/D_0>6 [86]. For lesions that are closer together, the overall energy loss is reduced, since energy diffusion in the expanding jet is limited by the distal lesion and flow tends to remain more laminar [61]. Steady flow studies have shown that if a severe lesion is closely (S/D_0 =2) followed by a mild or moderate stenosis, the overall pressure drop was even less than that across the single severe stenosis [87]. If the upstream stenosis is compliant, increasing the severity of the downstream stenosis in a coronary artery can lead to expansion of the upstream stenosis lumen area, thereby decreasing its hemodynamic effect and increasing flow through both lesions [88, 89].

Selecting the most appropriate stenosis of serial lesions to be dilated is challenging. A method to predict the theoretical pressure drop across the remaining individual lesion after virtual stepwise revascularization is complicated and involves obtaining a wedge pressure requiring balloon inflation [90]. In the case of a left main stenosis in the presence of a downstream left anterior or circumflex lesion, it was proposed to measure distal pressure in the uninvolved epicardial artery instead [91]. However, both methods assume a constant hyperemic microvascular resistance regardless of distending pressure to the downstream myocardial bed, and the effect of distance between the lesions on mutual interaction was not investigated. A practical approach to identify the culprit lesion may be to determine sudden steps in pressure gradient by pressure wire pullback along the length of a coronary artery during hyperemia [92].

In summary, the overall effect of serial stenoses not only depends on the severity of the stenoses and the distance between them but also on the sequence of lesion severities, on stenosis compliance, and on flow. Clearly, more studies are needed in this area, but it is certain that multiple noncritical stenoses can cause a significant pressure loss, especially in the presence of underlying diffuse narrowing.

Diffuse disease The importance of diffuse coronary artery disease underlying a focal stenosis has long been recognized [93] and continues to be an active focus of research attention [94, 95]. A tandem development of focal and diffuse coronary artery disease is common and is associated with an increased risk of coronary events [17, 95, 96]. Recent studies using computed tomography imaging have shown that the cumulative plaque burden proximal to a focal stenosis plays an important role in determining the functional significance of that stenosis [97, 98].

Detection of diffuse disease by conventional angiographic imaging remains a problem for interventional cardiologists. The true extent of plaque accumulation cannot be appreciated by luminal angiography that may show smooth vessels, falsely suggesting the absence of atherosclerotic disease, and errors in angiographic assessment of plaque burden are exacerbated by the frequent occurrence of eccentric plaques that may present angiographically as a marginally narrowed circular lumen [99]. Yet the absence of focal disease does not imply the absence of increased flow resistance. Diffuse segmental narrowing can lead to substantial loss in distal perfusion pressure [100, 101] and can conceptually be modeled as a uniform relative reduction in normal segmental diameter with or without an overlaying focal obstruction [102]. Normal coronary artery size in humans is not easy to assess [103, 104]. Several approaches have employed length-area relations based on scaling laws that relate the size of the coronary tree to regional perfused mass via cumulative distal artery branch length [105, 106] or tried to assess the size of normal vessels via bifurcation analysis, where deviation from normal scaling law patterns can reveal the severity of diffuse disease [107–109]. Based on this approach, the extent of diffuse disease in the epicardial coronary artery tree of patients with metabolic syndrome was reflected by a 28 % decrease of mean cross-sectional area along the entire epicardial coronary artery tree and an 18% decrease of the sum of intravascular volume as a result of reduced cross-sectional area in distal coronary arteries [108].

Recapitulating, the hemodynamics of an epicardial stenosis can be summarized as follows:

1. Stenosis pressure drop (and therefore flow through the vessel) is influenced by stenosis geometry (shape of converging and diverging section, plaque location, length, lumen area of the stenosis, and lumen area of the vessel), velocity, blood viscosity and density, and blood flow waveform. Of these, the most important factors are flow velocity and minimum stenosis diameter.
2. The pressure drop varies nonlinearly with flow velocity, and the resistance of a stenosis is therefore not constant. For a fixed geometry, stenosis resistance increases linearly with velocity. In this regard, it should be recognized that microvascular resistance influences stenosis hemodynamics via its direct influence on flow velocity.
3. The major geometric factor influencing the pressure drop is the reduction in lumen area. This effect is relatively small for mild lesions, but escalates nonlinearly with increasing stenosis severity, where even a small worsening in stenosis diameter causes a steep rise in pressure drop.
4. Stenosis shape and lumen eccentricity do not strongly affect the pressure drop for moderate to severe lesions for which lumen reduction dominates. However, in case of partially compliant lesions (compliant plaque or an arc of flexible wall circumference), dynamic behavior can be introduced by small changes in effective lesion diameter with decreasing distending pressure, e.g., at elevated flow rates (passive) or induced by changes in tone (active).
5. The effect of multiple stenoses depends on the severity of the lesions, sequence of different severities, spacing between the lesions, and flow. If the distal lesion is close enough to the proximal one, it interferes with the expanding jet emerging from the upstream stenosis, thereby reducing its pressure loss. Based on experimental findings, sequential lesions can be regarded as independent (overall pressure drop is determined by the sum of individual lesions) when the distance between the lesions is greater than 6 times the adjacent vessel diameter.
6. Diffuse coronary artery disease underlying a focal lumen obstruction is common and independently modulates the physiological effect of an epicardial stenosis.

1.4 Distal Perfusion Beyond the Epicardial Lesion: Integrated Measures of Physiological Stenosis Severity

Considering that flow velocity is a major physiological determinant of epicardial stenosis hemodynamics for any given driving pressure, the level of microvascular resistance at the time of measurement is of paramount importance. After all, the value of basal and maximal flow during physiological lesion assessment determines the position along the stenosis ΔP-Q relationship, and clinically relevant functional parameters are derived from these values.

The power of conveying stenosis hemodynamics in terms of combined pressure and flow velocity information is further depicted in Fig. 1.14 showing stenosis ΔP-Q relationships for a selection of clinical cases. Data were obtained during a diagnostic procedure with intracoronary adenosine administration in coronary arteries of six patients with various degrees of anatomical stenosis severity.

In line with observations and simulations by others [94, 102], it becomes clear that percent diameter reduction alone is not a defining measure for the functional severity of a lesion. As shown in Fig. 1.14a, two lesions of 55 % DS (light blue and green) have very different ΔP-Q relationships (due to different diameters of the stenosed coronary vessel), whereas the fluid dynamic relationship of the 50 % DS (orange) is on the same curve as that of a 55 % DS (shown in green), albeit at a much lower flow velocity range. When pressure gradient is expressed in terms of aortic pressure ($1-\Delta P/P_a = P_d/P_a$), it can be seen

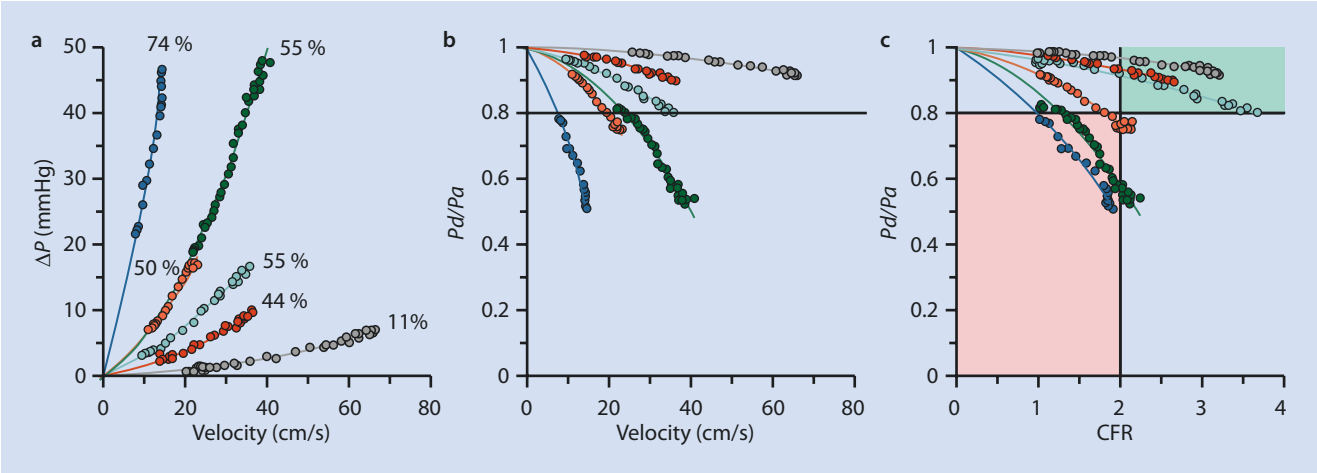

Fig. 1.14 Combined pressure and velocity measurements during the hyperemic response to intracoronary adenosine. **a** Examples of pressure drop (ΔP)-velocity relations obtained for different stenosis severities in coronary arteries of patients. It is clear that percent diameter reduction alone is not a defining measure of hemodynamic severity. **b** When the ratio of distal (P_d) to proximal (P_a) pressure is shown on the y-axis, three lesions cross the threshold of 0.8 for fractional flow reserve at maximal flow during hyperemia. **c** Expressing the x-axis in terms of coronary flow reserve (CFR) reveals that only the most severe lesion stays below the threshold value of 2.0. The vasodilatory capacity of all other lesions was sufficient to sustain an adequate flow reserve

(Fig. 1.14b) that three lesions cross the threshold of 0.8 for fractional flow reserve. Two of these lesions reduce distal perfusion pressure during vasodilation to about half of the aortic input pressure, although flow velocity for the 55 % DS (green) is much higher than for the 74 % DS. As discussed earlier, a decline in distending pressure of the dilated microvascular bed to low values will invariably lead to a passive diameter reduction of the relaxed microvessels, with consequentially (Poiseuille losses) an enhanced microvascular resistance compared to more normotensive distension pressures [30]. Finally, expressing hyperemic velocity as a multiple of basal velocity (Fig. 1.14c) reveals that only the most severe stenosis falls below the established cutoff value of 2.0 for coronary flow reserve. Obviously, other factors than percent diameter stenosis are influential in determining the physiological impact of a stenosis.

Note that the green 55 % DS was associated with the lowest hyperemic microvascular resistance (1.39 mmHg·cm^{-1}·s), suggesting that the vasodilatory capacity of that microvascular bed was sufficient to sustain an adequate flow reserve. In contrast, the hyperemic microvascular resistance distal to the 50 % DS (orange) was much higher (2.19 mmHg·cm^{-1}·s), which is corroborated by the low maximal velocity that was achieved. It is not known to which extent this HMR may reflect microvascular dysfunction, but removing the stenosis might still help this patient. Hoffman therefore proposed that threshold values for Pd/Pa should not be fixed, but should vary with the individual level of peripheral coronary resistance [32]. The same should likely be applied to flow velocity reserve, and this view was expressed in recommendations to adopt more integrated physiological measures [96, 110].

Coronary stenosis physiology from anatomy Despite the established fluid dynamic equations of an arterial stenosis, prediction of physiology from anatomy alone is subject to much scatter that limits agreement with observed functional indices in individual patients [17, 94]. The dissociation of anatomic and functional measures of stenosis severity is due not only to diffuse atherosclerosis but also to the influence of microvascular function that ultimately determines maximal flow and, hence, pressure gradient. Additionally, even quantitative angiography or computed tomography cannot assess stenosis dimensions with an accuracy that is adequate to enter with a fourth power relationship into the fluid dynamic equations [94]. Studies employing 3D computational fluid dynamics (CFD) assume population-based values for coupled reduced-order models describing the inlet and outlet boundary conditions of epicardial coronary arteries. Parameters of normal coronary models are applied to diseased models. Resistance values of the downstream vasculature are assumed to be dictated by their own anatomy (as derived from images) rather than by the upstream stenosis (which also modulates distal pressure and, hence, downstream resistance) [111]. Therefore, the application of classical fluid dynamic principles and 3D CFD as a tool for the patient-specific prediction of physiological stenosis severity from image-derived stenosis geometry still faces many challenges and limitations [94, 112].

Coronary flow as physiological parameter of choice The concept of "critical reduction in flow capacity" was introduced to aid in clinical interpretation of physiological severity [113]. The premise of this concept is that actual pressure and flow levels measured in epicardial vessels represent a continuum that is modulated by many external factors beyond the focal stenosis, including vasodilatory capacity (microvascular dysfunction), stress level, perfused mass (which is not accounted for with invasive measurements), vessel dimensions (diffuse disease), and distending pressure (input and distal pressure), as well as active and passive impeding mechanisms. A comprehensive approach termed "coronary flow capacity" was proposed by

Johnson, Gould, and colleagues [17, 114] that produces a 2D colored "physiological" scatterplot which takes into account both regional flow reserve and maximum stress flow (in ml/min/g) obtained by positron emission tomography as measures reflecting physiological stenosis severity, diffuse disease, and microvascular function. These data can be superimposed on left ventricular topographical depictions to yield a color-coded spatial distribution of coronary flow capacity. This concept has been "translated" to a "global" flow capacity map based on invasive measurements of flow velocity that also places the focus on the importance of coronary flow impairment for physiology-based decision-making in ischemic heart disease [115].

In conclusion, the hemodynamic characteristics of a coronary stenosis are governed by fluid dynamic laws that describe the quadratic relationship between pressure gradient and flow, based on (potentially variable) stenosis geometry and the rheological properties of blood. A coronary stenosis is proximally located in an epicardial curved, compliant, and moving vessel, with a downstream vascular network comprised of elastic branches whose resistance to flow is affected by active (tone) and passive (vasodilated) dimensional changes. This network is embedded in a continuously beating muscle that intrinsically regulates local myocardial perfusion based on oxygen demand at rest and during stress. All involved components can separately or together be diseased and malfunctioning to variable degrees. The physiological impact of an epicardial stenosis on perfusion impairment, therefore, derives from complex physical, biological, and pathophysiological interactions. Binary thresholding based on population-derived cutoff values of isolated epicardial physiological measurements obtained under pharmacologically simulated stress conditions should evolve toward integrating the accessible diagnostic information on multiple, individual factors of coronary artery disease into quantifiable criteria to optimize interventional decisions [116].

References

1. Fulton WF. The dynamic factor in enlargement of coronary arterial anastomoses, and paradoxical changes in the subendocardial plexus. Br Heart J. 1964;26:39–50.
2. Wusten B, Buss DD, Deist H, Schaper W. Dilatory capacity of the coronary circulation and its correlation to the arterial vasculature in the canine left ventricle. Basic Res Cardiol. 1977;72(6):636–50.
3. Spaan JAE, Ter Wee R, Van Teeffelen JWGE, Streekstra G, Siebes M, Kolyva C, et al. Visualisation of intramural coronary vasculature by an imaging cryomicrotome suggests compartmentalisation of myocardial perfusion areas. Med Biol Eng Comput. 2005;43(4):431–5.
4. van Horssen P, van den Wijngaard JP, Brandt M, Hoefer IE, Spaan JA, Siebes M. Perfusion territories subtended by penetrating coronary arteries increase in size and decrease in number towards the subendocardium. Am J Physiol Heart Circ Physiol. 2014;306(4):H496–504.
5. Hanley FL, Messina LM, Grattan MT, Hoffman JIE. The effect of coronary inflow pressure on coronary vascular resistance in the isolated dog heart. Circ Res. 1984;54(6):760–72.
6. Kanatsuka H, Ashikawa K, Komaru T, Suzuki T, Takishima T. Diameter change and pressure-red blood cell velocity relations in coronary microvessels during long diastoles in the canine left ventricle. Circ Res. 1990;66:503–10.
7. Marcus M, Chilian W, Kanatsuka H, Dellsperger K, Eastham C, Lamping K. Understanding the coronary circulation through studies at the microvascular level. Circulation. 1990;82(1):1–7.
8. Mosher P, Ross Jr J, McFate PA, Shaw RF. Control of coronary blood flow by an autoregulatory mechanism. Circ Res. 1964;14:250–9.
9. Canty Jr JM. Coronary pressure-function and steady-state pressure-flow relations during autoregulation in the unanesthetized dog. Circ Res. 1988;63(4):821–36.
10. Duncker DJ, Koller A, Merkus D, Canty Jr JM. Regulation of coronary blood flow in health and ischemic heart disease. Prog Cardiovasc Dis. 2015;57(5):409–22.
11. Chilian WM, Layne SM, Klausner EC, Eastham CL, Marcus ML. Redistribution of coronary microvascular resistance produced by dipyridamole. Am J Physiol Heart Circ Physiol. 1989;256(2 Pt 2):H383–90.
12. Uren NG, Melin JA, De Bruyne B, Wijns W, Baudhuin T, Camici PG. Relation between myocardial blood flow and the severity of coronary-artery stenosis. N Engl J Med. 1994;330(25):1782–8.
13. Marcus ML, Doty DB, Hiratzka LF, Wright CB, Eastham CL. Decreased coronary reserve: a mechanism for angina pectoris in patients with aortic stenosis and normal coronary arteries. N Engl J Med. 1982;307(22):1362–6.
14. Wilson RF, Wyche K, Christensen BV, Zimmer S, Laxson DD. Effects of adenosine on human coronary arterial circulation. Circulation. 1990;82(5):1595–606.
15. Windecker S, Allemann Y, Billinger M, Pohl T, Hutter D, Orsucci T, et al. Effect of endurance training on coronary artery size and function in healthy men: an invasive followup study. Am J Physiol Heart Circ Physiol. 2002;282(6):H2216–23.
16. Sdringola S, Johnson NP, Kirkeeide RL, Cid E, Gould KL. Impact of unexpected factors on quantitative myocardial perfusion and coronary flow reserve in young, asymptomatic volunteers. JACC Cardiovasc Imaging. 2011;4(4):402–12.
17. Gould KL, Johnson NP, Bateman TM, Beanlands RS, Bengel FM, Bober R, et al. Anatomic versus physiologic assessment of coronary artery disease. Role of coronary flow reserve, fractional flow reserve, and positron emission tomography imaging in revascularization decision-making. J Am Coll Cardiol. 2013;62(18):1639–53.
18. Chilian WM, Eastham CL, Marcus ML. Microvascular distribution of coronary vascular resistance in beating left ventricle. Am J Physiol Heart Circ Physiol. 1986;251(4):H779–88.
19. Hoffman JI, Spaan JA. Pressure-flow relations in coronary circulation. Physiol Rev. 1990;70(2):331–90.
20. Aldea GS, Mori H, Husseini WK, Austin RE, Hoffman JIE. Effects of increased pressure inside or outside ventricles on total and regional myocardial blood flow. Am J Physiol Heart Circ Physiol. 2000;279(6):H2927–38.
21. Komaru T, Kanatsuka H, Shirato K. Coronary microcirculation: physiology and pharmacology. Pharmacol Ther. 2000;86(3):217–61.
22. Spaan JAE. Coronary diastolic pressure-flow relation and zero flow pressure explained on the basis of intramyocardial compliance. Circ Res. 1985;56:293–309.
23. Spaan JAE. Mechanical determinants of myocardial perfusion. Basic Res Cardiol. 1995;90(2):89–102.
24. Cornelissen AJM, Dankelman J, VanBavel E, Stassen HG, Spaan JAE. Myogenic reactivity and resistance distribution in the coronary arterial tree: a model study. Am J Physiol Heart Circ Physiol. 2000;278(5):H1490–9.
25. Spaan J, Siebes M, Piek J. Coronary circulation and hemodynamics. In: Sperelakis N, Kurachi Y, Terzic A, Cohen M, editors. Heart physiology and pathophysiology. 4th ed. San Diego: Academic Press; 2001. p. 19–44.
26. Spaan JAE, Piek JJ, Hoffman JIE, Siebes M. Physiological basis of clinically used coronary hemodynamic indices. Circulation. 2006;113(3):446–55.
27. Heusch G. Adenosine and maximum coronary vasodilation in humans: myth and misconceptions in the assessment of coronary reserve. Basic Res Cardiol. 2010;105(1):1–5.

28. Downey JM, Kirk ES. Inhibition of coronary blood flow by a vascular waterfall. Circ Res. 1975;36:753–60.
29. Verhoeff B, Siebes M, Meuwissen M, Koch KT, De Winter RJ, Kearney D, et al. Changes of coronary microvascular resistance before and after percutaneous coronary intervention. Eur Heart J. 2003;24:328.
30. Indermuehle A, Vogel R, Meier P, Zbinden R, Seiler C. Myocardial blood volume and coronary resistance during and after coronary angioplasty. Am J Physiol Heart Circ Physiol. 2011;300(3):H1119–H24.
31. Duncker DJ, Zhang J, Bache RJ. Coronary pressure-flow relation in left ventricular hypertrophy. Importance of changes in back pressure versus changes in minimum resistance. Circ Res. 1993;72(3):579–87.
32. Hoffman JIE. Problems of coronary flow reserve. Ann Biomed Eng. 2000;28:884–96.
33. Uhlig PN, Baer RW, Vlahakes GJ, Hanley FL, Messina LM, Hoffman JI. Arterial and venous coronary pressure-flow relations in anesthetized dogs. Evidence for a vascular waterfall in epicardial coronary veins. Circ Res. 1984;55(2):238–48.
34. Watanabe J, Maruyama Y, Satoh S, Keitoku M, Takishima T. Effects of the pericardium on the diastolic left coronary pressure-flow relationship in the isolated dog heart. Circulation. 1987;75(3):670–5.
35. Messina LM, Hanley FL, Uhlig PN, Baer RW, Grattan MT, Hoffman JIE. Effects of pressure gradients between branches of the left coronary artery on the pressure axis intercept and the shape of steady state circumflex pressure-flow relations in dogs. Circ Res. 1985;56:11–9.
36. Scheel KW, Mass H, Williams SE. Collateral influence on pressure-flow characteristics of coronary circulation. Am J Physiol Heart Circ Physiol. 1989;257(3 Pt 2):H717–H25.
37. Spaan JAE. Coronary blood flow. mechanics, distribution, and control. Dordrecht: Kluwer; 1991. p. 14–6. 166–168.
38. Tune JD. Coronary circulation. San Rafael: Biota Publishing; 2015.
39. Spaan JAE, Breuls NPW, Laird JD. Diastolic-systolic flow differences are caused by intramyocardial pump action in the anesthetized dog. Circ Res. 1981;49:584–93.
40. Krams R, Sipkema P, Westerhof N. Varying elastance concept may explain coronary systolic flow impediment. Am J Physiol Heart Circ Physiol. 1989;257(5 Pt 2):H1471–9.
41. Westerhof N, Boer C, Lamberts RR, Sipkema P. Cross-talk between cardiac muscle and coronary vasculature. Physiol Rev. 2006;86(4): 1263–308.
42. Bruinsma P, Arts T, Dankelman J, Spaan JAE. Model of the coronary circulation based on pressure dependence of coronary resistance and compliance. Basic Res Cardiol. 1988;83(5):510–24.
43. Spaan JAE, Cornelissen AJM, Chan C, Dankelman J, Yin FC. Dynamics of flow, resistance, and intramural vascular volume in canine coronary circulation. Am J Physiol Heart Circ Physiol. 2000;278:H383–403.
44. Austin Jr RE, Aldea GS, Coggins DL, Flynn AE, Hoffman JI. Profound spatial heterogeneity of coronary reserve. Discordance between patterns of resting and maximal myocardial blood flow. Circ Res. 1990;67(2):319–31.
45. Hoffman JI. Heterogeneity of myocardial blood flow. Basic Res Cardiol. 1995;90(2):103–11.
46. Chareonthaitawee P, Kaufmann PA, Rimoldi O, Camici PG. Heterogeneity of resting and hyperemic myocardial blood flow in healthy humans. Cardiovasc Res. 2001;50:151–61.
47. van de Hoef TP, Nolte F, Rolandi MC, Piek JJ, van den Wijngaard JPHM, Spaan JAE, et al. Coronary pressure-flow relations as basis for the understanding of coronary physiology. J Mol Cell Cardiol. 2012;52(4):786–93.
48. Chilian WM. Microvascular pressures and resistances in the left ventricular subepicardium and subendocardium. Circ Res. 1991;69(3):561–70.
49. Bache R, Cobb F. Effect of maximal coronary vasodilation on transmural myocardial perfusion during tachycardia in the awake dog. Circ Res. 1977;41(5):648–53.
50. Flynn AE, Coggins DL, Goto M, Aldea GS, Austin RE, Doucette JW, et al. Does systolic subepicardial perfusion come from retrograde subendocardial flow? Am J Physiol Heart Circ Physiol. 1992;262(6):H1759–69.
51. Boudoulas H. Diastolic time: the forgotten dynamic factor. Implications for myocardial perfusion. Acta Cardiol. 1991;46(1):61–71.
52. Bache RJ, Schwartz JS. Effect of perfusion pressure distal to coronary stenosis on transmural myocardial blood flow. Circulation. 1982;65:928–32.
53. Merkus D, Vergroesen I, Hiramatsu O, Tachibana H, Nakamoto H, Toyota E, et al. Stenosis differentially affects subendocardial and subepicardial arterioles in vivo. Am J Physiol Heart Circ Physiol. 2001;280(4):H1674–82.
54. Ferro G, Duilio C, Spinelli L, Liucci GA, Mazza F, Indolfi C. Relation between diastolic perfusion time and coronary artery stenosis during stress-induced myocardial ischemia. Circulation. 1995;92(3):342–7.
55. Ferro G, Spinelli L, Duilio C, Spadafora M, Guarnaccia F, Condorelli M. Diastolic perfusion time at ischemic threshold in patients with stress-induced ischemia. Circulation. 1991;84(1):49–56.
56. Fokkema DS, VanTeeffelen JWGE, Dekker S, Vergroesen I, Reitsma JB, Spaan JAE. Diastolic time fraction as a determinant of subendocardial perfusion. Am J Physiol Heart Circ Physiol. 2005;288(5):H2450–6.
57. Merkus D, Kajiya F, Vink H, Vergroesen I, Dankelman J, Goto M, et al. Prolonged diastolic time fraction protects myocardial perfusion when coronary blood flow is reduced. Circulation. 1999;100(1):75–81.
58. Roschke EJ, Back LH. The influence of upstream conditions on flow reattachment lengths downstream of an abrupt circular channel expansion. J Biomech. 1976;9(7):481–3.
59. Kirkeeide RL, Young DF, Cholvin NR. Wall vibrations induced by flow through simulated stenoses in models and arteries. J Biomech. 1977;10(7):431–7.
60. Seeley BD, Young DF. Effect of geometry on pressure losses across models of arterial stenoses. J Biomech. 1976;9:439–48.
61. Young DF. Fluid mechanics of arterial stenoses. J Biomech Eng. 1979;101(3):157–75.
62. Young DF, Cholvin NR, Kirkeeide RL, Roth AC. Hemodynamics of arterial stenoses at elevated flow rates. Circ Res. 1977;41(1):99–107.
63. Siebes M, Tjajahdi I, Gottwik M, Schlepper M. Influence of elliptical and eccentric area reduction on the pressure drop across stenoses. Z Kardiol. 1984;73:59.
64. Kirkeeide RL. Coronary obstructions, morphology and physiologic significance. In: Reiber JHC, Serruys PW, editors. Quantitative coronary arteriography. Dordrecht: Kluwer Academic Publishers; 1991. p. 229–44.
65. Huo Y, Svendsen M, Choy JS, Zhang Z-D, Kassab GS. A validated predictive model of coronary fractional flow reserve. J R Soc Interface. 2012;9(71):1325–38.
66. Gould KL. Pressure-flow characteristics of coronary stenoses in unsedated dogs at rest and during coronary vasodilation. Circ Res. 1978;43(2):242–53.
67. Siebes M, Verhoeff BJ, Meuwissen M, de Winter RJ, Spaan JAE, Piek JJ. Single-wire pressure and flow velocity measurement to quantify coronary stenosis hemodynamics and effects of percutaneous interventions. Circulation. 2004;109(6):756–62.
68. Nolte F, van de Hoef TP, de Klerk W, Baan Jr J, Lockie TP, Spaan JA, et al. Functional coronary stenosis severity assessed from the mean pressure gradient-velocity relationship obtained by contrast medium-induced submaximal hyperaemia. EuroIntervention. 2014;10(3):320–8.
69. Marques KMJ, Spruijt HJ, Boer C, Westerhof N, Visser CA, Visser FC. The diastolic flow-pressure gradient relation in coronary stenoses in humans. J Am Coll Cardiol. 2002;39(10):1630–6.
70. Vlodaver Z, Edwards JW. Pathology of coronary atherosclerosis. Prog Cardiovasc Dis. 1971;14:256–74.
71. Freudenberg H, Lichtlen PR. The normal wall segment in coronary stenoses – a postmortem study. Z Kardiol. 1981;70:863–9.
72. Waller BF. The eccentric coronary atherosclerotic plaque: morphologic observations and clinical relevance. Clin Cardiol. 1989;12(1):14–20.
73. Jeremias A, Huegel H, Lee DP, Hassan A, Wolf A, Yeung AC, et al. Spatial orientation of atherosclerotic plaque in non-branching coronary artery segments. Atherosclerosis. 2000;152(1):209–15.

74. Tang D, Yang C, Zheng J, Woodard PK, Saffitz JE, Petruccelli JD, et al. Local maximal stress hypothesis and computational plaque vulnerability index for atherosclerotic plaque assessment. Ann Biomed Eng. 2005;33(12):1789–801.
75. Sadat U, Teng Z, Gillard JH. Biomechanical structural stresses of atherosclerotic plaques. Expert Rev Cardiovasc Ther. 2010;8(10):1469–81.
76. Akyildiz AC, Speelman L, Gijsen FJ. Mechanical properties of human atherosclerotic intima tissue. J Biomech. 2014;47(4):773–83.
77. Ohayon J, Finet G, Le Floc'h S, Cloutier G, Gharib AM, Heroux J, et al. Biomechanics of atherosclerotic coronary plaque: site, stability and in vivo elasticity modeling. Ann Biomed Eng. 2014;42(2):269–79.
78. Logan SE. On the fluid mechanics of human coronary artery stenosis. IEEE Trans Biomed Eng. 1975;22(4):327–34.
79. Walinsky P, Santamore WP, Wiener L, Brest A. Dynamic changes in the haemodynamic severity of coronary artery stenosis in a canine model. Cardiovasc Res. 1979;13:113–8.
80. Schwartz JS, Carlyle PF, Cohn JN. Effect of coronary arterial pressure on coronary stenosis resistance. Circulation. 1980;61:70–6.
81. Gould KL. Dynamic coronary stenosis. Am J Cardiol. 1980;45(2):286–92.
82. Santamore WP, Kent RL, Carey RA, Bove AA. Synergistic effects of pressure, distal resistance, and vasoconstriction on stenosis. Am J Physiol Heart Circ Physiol. 1982;243(2):H236–42.
83. Brown BG, Lee AB, Bolson EL, Dodge HT. Reflex constriction of significant coronary stenosis as a mechanism contributing to ischemic left ventricular dysfunction during isometric exercise. Circulation. 1984;70(1):18–24.
84. Schwartz JS, Bache RJ. Effect of arteriolar dilation on coronary artery diameter distal to coronary stenoses. Am J Physiol Heart Circ Physiol. 1985;249(5 Pt 2):H981–8.
85. Siebes M, Campbell CS, D'Argenio DZ. Fluid dynamics of a partially collapsible stenosis in a flow model of the coronary circulation. J Biomech Eng. 1996;118(4):489–97.
86. Siebes M, Gottwik MG, Schlepper M. Experimental studies of the pressure drop across serial stenoses. Proceeding World Congress on Medical Physics and Biomedical Engineering. Hamburg: IFMBE; 1982. p. 2. 47.
87. Siebes M, Gottwik MG, Schlepper M. Hemodynamic effect of sequence and severity of serial stenoses. J Am Coll Cardiol. 1983;1(2):684.
88. Schwartz JS. Interaction of compliant coronary stenoses in series in a canine model. Am J Med Sci. 1985;289(5):192–9.
89. John B, Siebes M. Effects of stenosis compliance on flow through sequential stenoses. Adv Bioeng Am Soc Mech Eng. 1992;BED-22:383–6.
90. Pijls NHJ, De Bruyne B, Bech GJW, Liistro F, Heyndrickx GR, Bonnier HJRM, et al. Coronary pressure measurement to assess the hemodynamic significance of serial stenoses within one coronary artery: validation in humans. Circulation. 2000;102(19):2371–7.
91. Fearon WF, Yong AS, Lenders G, Toth GG, Dao C, Daniels DV, et al. The impact of downstream coronary stenosis on fractional flow reserve assessment of intermediate left main coronary artery diseasehuman validation. J Am Coll Cardiol Intv. 2015;8(3):398–403.
92. Kim H-L, Koo B-K, Nam C-W, Doh J-H, Kim J-H, Yang H-M, et al. Clinical and physiological outcomes of fractional flow reserve-guided percutaneous coronary intervention in patients with serial stenoses within one coronary artery. JACC Cardiovasc Interv. 2012;5(10):1013–8.
93. Marcus ML, Harrison DG, White CW, McPherson DD, Wilson RF, Kerber RE. Assessing the physiologic significance of coronary obstructions in patients: importance of diffuse undetected atherosclerosis. Prog Cardiovasc Dis. 1988;31(1):39–56.
94. Johnson NP, Kirkeeide RL, Gould KL. Coronary anatomy to predict physiology: fundamental limits. Circ Cardiovasc Imaging. 2013;6(5):817–32.
95. Gould KL, Johnson NP. Physiologic severity of diffuse coronary artery disease: hidden high risk. Circulation. 2015;131(1):4–6.
96. Gould KL, Johnson NP, Kaul S, Kirkeeide RL, Mintz GS, Rentrop KP, et al. Patient selection for elective revascularization to reduce myocardial infarction and mortality: new lessons from randomized trials, coronary physiology, and statistics. Circ Cardiovasc Imaging. 2015;8(5):e003099.
97. Nakazato R, Shalev A, Doh JH, Koo BK, Gransar H, Gomez MJ, et al. Aggregate plaque volume by coronary computed tomography angiography is superior and incremental to luminal narrowing for diagnosis of ischemic lesions of intermediate stenosis severity. J Am Coll Cardiol. 2013;62(5):460–7.
98. Abd TT, George RT. Association of coronary plaque burden with fractional flow reserve: should we keep attempting to derive physiology from anatomy? Cardiovasc Diagn Ther. 2015;5(1):67–70.
99. Narula J, Nakano M, Virmani R, Kolodgie FD, Petersen R, Newcomb R, et al. Histopathologic characteristics of atherosclerotic coronary disease and implications of the findings for the invasive and noninvasive detection of vulnerable plaques. J Am Coll Cardiol. 2013;61(10):1041–51.
100. De Bruyne B, Hersbach F, Pijls NHJ, Bartunek J, Bech J-W, Heyndrickx GR, et al. Abnormal epicardial coronary resistance in patients with diffuse atherosclerosis but "normal" coronary angiography. Circulation. 2001;104(20):2401–6.
101. Back LH, Cho YI, Crawford DW, Cuffel RF. Effect of mild atherosclerosis on flow resistance in a coronary artery casting of man. J Biomech Eng. 1984;106:48–53.
102. Johnson NP, Kirkeeide RL, Gould KL. Is discordance of coronary flow reserve and fractional flow reserve due to methodology or clinically relevant coronary pathophysiology? JACC Cardiovasc Imaging. 2012;5(2):193–202.
103. Dodge Jr J, Brown B, Bolson E, Dodge H. Lumen diameter of normal human coronary arteries. Influence of age, sex, anatomic variation, and left ventricular hypertrophy or dilation. Circulation. 1992;86(1):232–46.
104. Santamore WP, Bove AA. Why are arteries the size they are? J Appl Physiol. 2008;104(5):1259.
105. Seiler C, Kirkeeide RL, Gould KL. Basic structure-function relations of the epicardial coronary vascular tree. Basis of quantitative coronary arteriography for diffuse coronary artery disease. Circulation. 1992;85(6):1987–2003.
106. Gould KL, Nakagawa Y, Nakagawa K, Sdringola S, Hess MJ, Haynie M, et al. Frequency and clinical implications of fluid dynamically significant diffuse coronary artery disease manifest as graded, longitudinal, base-to-apex myocardial perfusion abnormalities by noninvasive positron emission tomography. Circulation. 2000;101(16):1931–54.
107. Choy JS, Kassab GS. Scaling of myocardial mass to flow and morphometry of coronary arteries. J Appl Physiol. 2008;104(5):1281–6.
108. Huo Y, Wischgoll T, Choy JS, Sola S, Navia JL, Teague SD, et al. CT-based diagnosis of diffuse coronary artery disease on the basis of scaling power laws. Radiology. 2013;268(3):694–701.
109. Kassab GS, Finet G. Anatomy and function relation in the coronary tree: from bifurcations to myocardial flow and mass. EuroIntervention. 2015;11(V):V13–V7.
110. Johnson NP, Toth GG, Lai D, Zhu H, Acar G, Agostoni P, et al. Prognostic value of fractional flow reserve: linking physiologic severity to clinical outcomes. J Am Coll Cardiol. 2014;64(16):1641–54.
111. Zhang JM, Zhong L, Su B, Wan M, Yap JS, Tham JP, et al. Perspective on CFD studies of coronary artery disease lesions and hemodynamics: a review. Int J Numer Method Biomed Eng. 2014;30(6):659–80.
112. Morris PD, van de Vosse FN, Lawford PV, Hose DR, Gunn JP. "Virtual" (Computed) fractional flow reserve current challenges and limitations. JACC Cardiovasc Interv. 2015;8:1009–17.
113. Gould KL. Does coronary flow trump coronary anatomy? JACC Cardiovasc Imaging. 2009;2(8):1009–23.
114. Johnson NP, Gould KL. Integrating noninvasive absolute flow, coronary flow reserve, and ischemic thresholds into a comprehensive map of physiological severity. JACC Cardiovasc Imaging. 2012;5(4):430–40.
115. van de Hoef TP, Siebes M, Spaan JA, Piek JJ. Fundamentals in clinical coronary physiology: why coronary flow is more important than coronary pressure. Eur Heart J. 2015; 36(47):3312-9.
116. Gould KL, Johnson NP. Physiologic stenosis severity, binary thinking, revascularization, and "hidden reality". Circ Cardiovasc Imaging. 2015;8(1):e002970.

Pathological Changes in the Coronary Circulation

Contents